

Lorentz violation and momentum-space geometric phases

V. Alan Kostelecký^{1,2}, Ralf Lehnert^{1,2}, Marco Schreck³, and Babak Seradjeh^{1,2,4}

¹*Department of Physics, Indiana University, Bloomington, Indiana 47405, USA*

²*Indiana University Center for Spacetime Symmetries, Bloomington, Indiana 47405, USA*

³*Departamento de Física, Universidade Federal do Maranhão,*

Campus Universitário do Bacanga, São Luís (MA), 65085-580, Brazil

⁴*Quantum Science and Engineering Center, Indiana University, Bloomington, Indiana 47405, USA*

Geometric phases can manifest when a relativistic quantum particle moves cyclically along a loop in parameter space. The phase can be affected by the presence of a background field and can be accompanied by nontrivial topological features. The appearance of adiabatic geometric phases in momentum space is demonstrated for a Lorentz-violating Weyl fermion, where the role of the background is played by the coefficients for Lorentz violation. As explicit examples, the Berry curvature and the first Chern number are derived for two cases with large Lorentz violation, one incorporating CPT violation and one preserving CPT symmetry. Some alternative topological invariants are also obtained. In certain scenarios with large Lorentz violation, the physical vacuum is associated with a topological phase.

I. INTRODUCTION

As a quantum state evolves, it develops a dynamical phase governed by a hamiltonian. The state can also acquire an additional observable geometric phase when parameters of the system undergo an adiabatic change along a closed curve in parameter space. This additional phase, known as the Pancharatnam-Berry phase or Berry phase [1, 2], has an interpretation as the holonomy of the curve in the U(1) bundle over the parameter space [3], and in a nontrivial bundle the phase is associated with topological invariants. Geometric phases are known to appear in other scenarios, such as non-adiabatic motion [4] or modified boundary conditions [5], and the appearance of geometric and topological phases in physics is now widespread [6–8].

The parameter space associated with the Berry phase can be spanned by quantities such as applied fields that appear in the hamiltonian of the system. Alternatively, the parameter space can be taken as three-dimensional momentum space \mathcal{P}_3 , and the wave function at position \mathbf{r} written as $\exp(i\mathbf{p} \cdot \mathbf{r})|\psi(\mathbf{p})\rangle$ for $\mathbf{p} \in \mathcal{P}_3$. The quantum state $|\psi(\mathbf{p})\rangle$ resides in the U(1) bundle over \mathcal{P}_3 , and it measures the deviation of the wave function from a plane wave as determined from the structure of the hamiltonian and the boundary conditions. Adiabatic evolution of the wave function around a closed curve in \mathcal{P}_3 can then generate a nontrivial momentum-space geometric phase.

The focus of this work is the effect on the momentum-space geometric phase of a relativistic fermion moving in a generic background. This physical scenario is central to theoretical and experimental studies of Lorentz violation. In the context of fundamental physics, for example, Lorentz violation represents a prospective signal for an underlying unified theory at the Planck scale such as strings [9, 10]. Tiny corrections to known physics can be incorporated using effective field theory [11], yielding a framework known as the Standard-Model Extension (SME) that describes general effects of Lorentz violation in particle physics and gravity [12–16]. As another exam-

ple, in condensed-matter physics the treatment of Weyl and Dirac semimetals is closely analogous to the effective field theory of Lorentz-violating fermions. The dynamical behavior of a quasiparticle excitation in certain regions of the semimetal band structure displays measurable deviations from emergent Lorentz invariance [17–21], and Lorentz-violating effective field theory can be used to describe the associated physics [22–25].

In the SME, each Lorentz-violating term in the Lagrange density is accompanied by a coefficient that acts as a background controlling observable effects. The coefficient can appear in the quantum hamiltonian and hence can modify the geometric phase of the fermion when it moves adiabatically along a curve in momentum space, even when the coefficient itself is homogeneous and constant in time. The general effective field theory for a Lorentz-violating fermion thus represents an ideal framework for investigating the background dependence of momentum-space geometric phases. Here, we explore this background dependence by investigating two examples that are widely used in studies of Lorentz-violating physics. One has a background involving a coefficient b_μ for Lorentz violation that incorporates also violation of the product CPT of charge conjugation C, parity inversion P, and time reversal T. The background in the second example involves a coefficient $d_{\mu\nu}$ for Lorentz violation that preserves CPT symmetry.

The relationship between the background and the momentum-space geometric phase is of interest in its own right. However, it can have particular relevance for scenarios with large Lorentz violation, where perturbative techniques are inadequate to understand the physics. These scenarios arise either when the coefficients for Lorentz violation are intrinsically large in a chosen frame or when they are small in one frame but a highly boosted frame is adopted. Identifying a consistent framework for treating these scenarios is known as the concordance problem [26]. For a fermion in the presence of Lorentz violation governed by dominant operators of mass dimension three, a generic physical solution

to the concordance problem has recently been demonstrated using thermodynamic arguments and the properties of semimetals [24]. In this picture, the physical vacuum at zero temperature contains particles with negative energies, paralleling the situation in the ground state of certain Weyl semimetals [22, 27, 28]. These particles endow the physical vacuum with a momentum-space geometric phase that has topological properties determined by the background.

The momentum-space geometric phases studied in this work involve relativistic dispersions for time-independent and spatially homogeneous backgrounds, including ones with large Lorentz violation and a nontrivial physical vacuum. Other types of geometric phases associated with Lorentz violation can also be considered. For example, in the limit of nonrelativistic motion and perturbative Lorentz violation, the spatial components b_j of the coefficient b_μ couple to the fermion spin like a background magnetic field [29], so the canonical illustration of the Berry phase arising when a nonrelativistic spin evolves in an adiabatically varying magnetic field [2] therefore maps directly to this scenario. The case with a perturbative coefficient $d_{\mu\nu}$ has been studied by Casana *et al.* [30], who show that the corresponding nonrelativistic hamiltonian induces an Aharonov-Anandan phase [4] in the wave function of an electron moving on a one-dimensional ring. Examples of geometric phases for nonrelativistic fermion motion in the presence of nonminimal SME operators of dimensions five or more coupled to the electromagnetic field have been extensively studied as well [31–41].

The paper is organized as follows. Basic results are outlined for the Lorentz-violating fermions with coefficients b_μ and $d_{\mu\nu}$ in Sec. II A and for momentum-space geometric phases in Sec. II B. The derivations of the momentum-space geometric phases and the associated Berry curvatures and first Chern numbers in the presence of b_μ are discussed in Sec. III, while the analogous results are obtained for $d_{\mu\nu}$ in Sec. IV. Some alternative topological invariants are considered in Sec. V. We conclude in Sec. VI. Our conventions incorporate natural units with $\hbar = c = 1$ unless otherwise stated. Greek letters are adopted for Lorentz indices, and Latin letters represent spatial indices. The Minkowski metric $\eta_{\mu\nu}$ has negative signature, and the Dirac matrices γ^μ satisfy the Clifford algebra $\{\gamma^\mu, \gamma^\nu\} = 2\eta^{\mu\nu}$, with $\gamma_5 := i\gamma^0\gamma^1\gamma^2\gamma^3$.

II. BASICS

A. Lorentz-violating fermions

The full SME incorporates general background couplings to all fields appearing in the Standard Model and General Relativity [12–16]. Numerous experimental studies of these backgrounds have been performed in recent years, in some cases achieving Planck-scale sensitivities or beyond to the coefficients for Lorentz violation [42]. Reviews of the SME can be found, for example,

in Refs. [43–48]. For the purposes of the present work, we limit attention to a Lorentz-violating fermion moving in flat spacetime in the presence of backgrounds that are time independent and spatially homogeneous.

Our focus here is on two specific scenarios, one involving a coefficient b_μ and the other a coefficient $d_{\mu\nu}$. Each coefficient modifies the hyperboloidal mass shell for a massive Dirac fermion or the standard light cone for a Weyl fermion. In both cases the modifications are spin dependent, so the spinor degrees of freedom in the energy eigenstates can play a significant role in the analysis. For b_μ the effects include CPT violation, but for $d_{\mu\nu}$ they are CPT invariant.

The action for a Dirac spinor field ψ of mass m_ψ coupled to the coefficient b_μ for Lorentz violation can be written as [13, 14, 26]

$$S_b = \int d^4x \frac{1}{2} \bar{\psi} (\gamma^\mu i\partial_\mu - m_\psi - b_\mu \gamma_5 \gamma^\mu) \psi + \text{h.c.}, \quad (1)$$

where $\bar{\psi} := \psi^\dagger \gamma^0$ as usual. Note that b_μ has mass dimension one in natural units. The properties of this action have been explored in the context of quantum field theory in fundamental physics [13, 25, 49–69] and in the contexts of classical mechanics and Finsler geometry [70–78]. The action S_b has also been widely studied as a phenomenological theory for Lorentz violation in electrons, protons, neutrons, and other fermions in atomic, nuclear, and particle physics and in astrophysics [79–116], while in condensed-matter physics it describes the band structures of certain Weyl semimetals [22, 23, 27, 28, 117–123].

The dimensionless coefficient $d_{\mu\nu}$ governs a Lorentz-violating operator similar to that for b_μ but containing an additional derivative. The corresponding action takes the form [13, 14, 26]

$$S_d = \int d^4x \frac{1}{2} \bar{\psi} (\gamma^\mu i\partial_\mu - m_\psi + d_{\mu\nu} \gamma_5 \gamma^\mu i\partial^\nu) \psi + \text{h.c.} \quad (2)$$

Features of this action have been investigated in quantum field theory [54, 58, 62, 65, 124–128], and constraints on the components of $d_{\mu\nu}$ have been obtained from experiments in several subfields [82, 88, 92, 93, 98, 101, 104, 115, 129–136]. Note that $d_{\mu\nu}$ has 16 components. However, the trace $\eta^{\mu\nu} d_{\mu\nu}$ is an observer scalar controlling only Lorentz-invariant effects, so in what follows we limit attention to the 15 nontrace components of $d_{\mu\nu}$.

In the action S_b , values of b_μ large compared to the fermion mass m_ψ represent large Lorentz violation and can be associated with qualitative changes to the physical vacuum [24]. For completeness, it is thus desirable to avoid the assumption of perturbative Lorentz violation when exploring the momentum-space geometric phases. We therefore choose to work here in the massless limit $m_\psi \rightarrow 0$, which ensures that the Lorentz violation is always large in the action S_b and simplifies some of the analysis for the action S_d . This limit retains physically meaningful Lorentz violation provided the fermion ψ is implicitly understood to have suitable interactions

obstructing any field redefinitions that could otherwise eliminate the coefficients for Lorentz violation [14]. These interactions leave unaffected our analysis of momentum-space geometric phases, which is based on the motion of particle states described by the quadratic actions S_b and S_d .

B. Momentum-space geometric phases

The momentum-space geometric phase of interest here arises when a quantum state vector $|\psi(\mathbf{p})\rangle$ in the Hilbert space undergoes adiabatic motion along a curve \mathcal{C} in three-dimensional momentum space \mathcal{P}_3 . In geometric terms, this motion can be understood as parallel transport in the $U(1)$ complex vector bundle of states over \mathcal{P}_3 . The parallel transport is described by the Berry connection 1-form, which in this case has three components given by

$$\mathcal{A}_\psi(\mathbf{p}) := i\langle\psi(\mathbf{p})|\nabla_{\mathbf{p}}|\psi(\mathbf{p})\rangle. \quad (3)$$

This connection is related to the position operator. In a crystalline solid, for example, \mathbf{p} can be taken as the lattice momentum with $|\psi(\mathbf{p})\rangle$ as the Bloch state, and the action of the position operator in the momentum space spanned by $\exp(i\mathbf{p}\cdot\mathbf{r})|\psi(\mathbf{p})\rangle$ then matches $i\nabla_{\mathbf{p}} + \mathcal{A}_\psi(\mathbf{p})$.

The Berry connection is unphysical because it changes under a gauge transformation of the wave function,

$$\psi(\mathbf{p}) \mapsto \psi'(\mathbf{p}) = \exp(i\alpha(\mathbf{p}))|\psi(\mathbf{p})\rangle, \quad (4a)$$

$$\mathcal{A}_\psi \mapsto \mathcal{A}_{\psi'} = \mathcal{A}_\psi - \nabla_{\mathbf{p}}\alpha, \quad (4b)$$

in analogy to the transformation of a $U(1)$ gauge field. However, integration of \mathcal{A}_ψ around a closed curve $\mathcal{C} \subset \mathcal{P}_3$ generates a momentum-space geometric phase $\Phi_{\mathcal{C}}$ that is gauge invariant modulo 2π ,

$$\Phi_{\mathcal{C}} = \oint_{\mathcal{C}} d\mathbf{l} \mathcal{A}_\psi(\mathbf{p}), \quad (5)$$

where $d\mathbf{l}$ is the line element along \mathcal{C} . The phase $\Phi_{\mathcal{C}}$ is nonzero whenever the holonomy of the curve \mathcal{C} is nontrivial. Another gauge-invariant quantity constructed from \mathcal{A}_ψ is the Berry curvature 2-form

$$\Omega_\psi(\mathbf{p}) := \nabla_{\mathbf{p}} \times \mathcal{A}_\psi(\mathbf{p}). \quad (6)$$

The analogy between \mathcal{A}_ψ and the $U(1)$ electromagnetic gauge potential implies that this curvature can be interpreted as an effective magnetic field in momentum space.

For each fermion mode of interest here, the dispersion $E = E(\mathbf{p})$ provides the eigenvalues of the hamiltonian for the quantum system. Extending momentum space \mathcal{P}_3 by the energy axis $p_0 = E$ implies that the dispersion can be viewed as specifying a three-dimensional subspace of the four-dimensional energy-momentum space \mathcal{P}_4 . The set of all hamiltonian eigenstates $|\psi_E(\mathbf{p})\rangle$ then gives rise to a bundle $P(U(1), \mathcal{P}_3)$. The various branches of the

dispersion can intersect or touch each other, indicating the presence of degeneracies. Degeneracies at an isolated point are particularly intriguing because the Berry curvature diverges at the point, representing a situation analogous to that of a magnetic monopole in electrodynamics. The corresponding connection possesses singularities along the Dirac string of the monopole. Consequently, no globally well-defined connection on $P(U(1), \mathcal{P}_3)$ exists. The obstruction can be characterized by a topological charge called the first Chern number, which can be computed by integrating the curvature over a closed surface S containing the monopole,

$$\oint_S dS \Omega_\psi(\mathbf{p}) \cdot \hat{\mathbf{n}} = 2\pi N_S. \quad (7)$$

In this equation, $\hat{\mathbf{n}}$ is a normal unit vector to S , dS is the surface element, and $N_S \in \mathbb{Z}$ is the topological charge. It follows that the total Berry curvature flux through a closed surface is quantized in units of 2π . In what follows, we take advantage of these topological properties to investigate the momentum-space geometric phases associated with the fermion actions S_b and S_d .

III. CPT-ODD CASE

This section explores the momentum-space geometric phases associated with the action S_b . We consider in turn scenarios with purely timelike, purely spacelike, and generic spacelike b_μ coefficients.

In the massless limit, the action S_b implies the modified Dirac equation

$$(\gamma^\mu \lambda_\mu - b_\mu \gamma_5 \gamma^\mu) \psi = 0, \quad (8)$$

where λ_μ is the wave four-vector. The Dirac equation can be written in Schrödinger form

$$H_b \psi = \lambda_0 \psi, \quad (9a)$$

$$H_b = H_0 + b_\mu \gamma^0 \gamma_5 \gamma^\mu, \quad (9b)$$

$$H_0 = -\gamma^0 \gamma^i \lambda_i, \quad (9c)$$

with a relativistic one-particle hamiltonian H_b for the b_μ theory, which is a modification of the standard Dirac hamiltonian H_0 .

A. Purely timelike coefficient

Consider a purely timelike b_μ , which is isotropic, with $b_0 > 0$. According to Eq. (9b), the relativistic hamiltonian of a free fermion modified by b_0 is then of the form

$$H_{\hat{b}} = H_0 - \hat{b} \gamma_5, \quad (10)$$

where $\hat{b} = b_0$ denotes the isotropic piece of b_μ [62]. In the following, all results are expressed in terms of the spatial-momentum 1-form $p = (p_i)$ where $p := |\mathbf{p}| = \sqrt{\sum_i p_i^2}$.

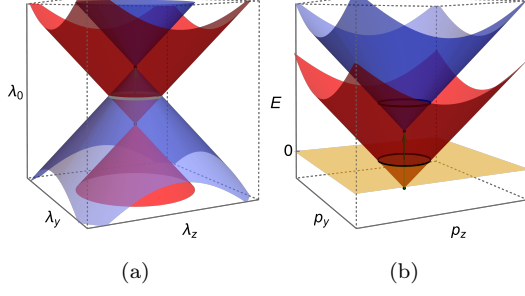


FIG. 1: Energy eigenvalues for the timelike case (a) before and (b) after reinterpretation.

Inspection reveals that $[H_0, H_b] = 0$, which implies that a common set of eigenvectors can be chosen for the standard Dirac hamiltonian and the isotropic modified hamiltonian. Like H_0 , H_b exhibits negative eigenvalues. In the presence of b_0 , however, the energy eigenvalues lie on Weyl cones shifted by b_0 along the positive and negative energy axes, respectively. The parts of these double cones below the Weyl points have either completely or primarily negative eigenvalues. The usual reinterpretation procedure reflects each part to the corresponding cone above the Weyl nodes. This yields

$$E_u^{(1,2)} = p \pm b_0, \quad (11a)$$

$$E_v^{(1,2)} = p \mp b_0. \quad (11b)$$

Here and in what follows, the labels (1) and (2) are correlated with the signs on the right-hand sides. Note that $E_u^{(2)}$ and $E_v^{(1)}$ dip below the $E = 0$ plane, whereupon negative energies are an inevitable consequence. This feature is one aspect of the concordance problem, for which a physical resolution is discussed in Ref. [24].

The energy eigenvalues of Eq. (9b) are illustrated in Fig. 1. In these plots, λ_μ is the wave 4-vector of a generic plane wave, whereas $p_\mu = (E, \mathbf{p})$ denotes the physical 4-momentum after reinterpretation. The yellow plane illustrates the Fermi level, and the black circles represent loops along which energy eigenstates can be parallel transported around the apices of the Weyl cones.

Applying the usual reinterpretation, the four spinor-valued energy eigenstates as functions of cartesian momentum-space coordinates can be cast into the form

$$|u^{(1,2)}(\mathbf{p})\rangle = |v^{(1,2)}(\mathbf{p})\rangle = n^{(1,2)} \begin{pmatrix} \pm(p_x - ip_y) \\ p \mp p_z \\ -(p_x - ip_y) \\ \mp p + p_z \end{pmatrix}, \quad (12a)$$

with the normalization factors

$$n^{(1,2)} = \frac{1}{2\sqrt{p(p \mp p_z)}}, \quad (12b)$$

such that

$$\langle u^{(1,2)} | u^{(1,2)} \rangle = 1 = \langle v^{(1,2)} | v^{(1,2)} \rangle. \quad (13)$$

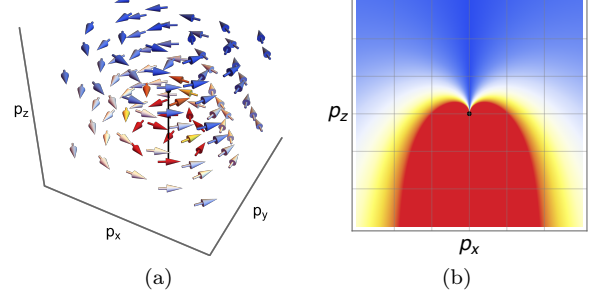


FIG. 2: (a) Berry connection vector field (16b), and (b) contour plot of its norm.

An alternative way of expressing these eigenstates is via spherical momentum-space coordinates (p, θ, ϕ) , where θ is the polar angle and ϕ is the azimuthal angle,

$$|u^{(1)}(\mathbf{p})\rangle = \frac{\exp(-i\phi)}{\sqrt{2}} \begin{pmatrix} \xi^{(1)} \\ -\xi^{(1)} \end{pmatrix} = |v^{(1)}(\mathbf{p})\rangle, \quad (14a)$$

$$|u^{(2)}(\mathbf{p})\rangle = \frac{1}{\sqrt{2}} \begin{pmatrix} \xi^{(2)} \\ \xi^{(2)} \end{pmatrix} = |v^{(2)}(\mathbf{p})\rangle, \quad (14b)$$

with the auxiliary two-component spinors

$$\xi^{(1)} = \xi^{(1)}(\theta, \phi) = \begin{pmatrix} \cos(\theta/2) \\ \sin(\theta/2) \exp(i\phi) \end{pmatrix}, \quad (15a)$$

$$\xi^{(2)} = \xi^{(2)}(\theta, \phi) = \begin{pmatrix} -\sin(\theta/2) \exp(-i\phi) \\ \cos(\theta/2) \end{pmatrix}. \quad (15b)$$

From the latter form we deduce that Eq. (12) represents helicity eigenstates. They correspond to the spinor solutions obtained in Ref. [13], modulo global phases.

In evaluating the momentum-space geometric phase using Eq. (5), the Dirac string is best revealed in spherical coordinates via Eqs. (14), (15). The eigenstates $|u^{(1)}\rangle$ and $|v^{(1)}\rangle$ have a ϕ -dependent limit when the negative p_z axis is approached, i.e., for $\theta \rightarrow \pi$. Thus, the limit of these states along the negative p_z axis is undefined. A similar behavior is observed for $|u^{(2)}\rangle$ and $|v^{(2)}\rangle$, but when we move toward the positive p_z axis, i.e., for $\theta \rightarrow 0$. This behavior is gauge dependent and changes under a gauge transformation. In cartesian and spherical coordinates, respectively, the Berry connection becomes

$$\mathcal{A}_u^{(1)} = \frac{1}{2p(p - p_z)} \begin{pmatrix} -p_y \\ p_x \\ 0 \end{pmatrix} = \frac{1}{2p} \cot\left(\frac{\theta}{2}\right) \hat{\phi} = \mathcal{A}_v^{(1)}, \quad (16a)$$

$$\mathcal{A}_u^{(2)} = \frac{1}{2p(p + p_z)} \begin{pmatrix} -p_y \\ p_x \\ 0 \end{pmatrix} = \frac{1}{2p} \tan\left(\frac{\theta}{2}\right) \hat{\phi} = \mathcal{A}_v^{(2)}, \quad (16b)$$

with the unit vector $\hat{\phi}$ tangential to circles of latitude of the sphere. The Dirac strings for $\mathcal{A}_{u,v}^{(1)}$ and $\mathcal{A}_{u,v}^{(2)}$ are evident when $\theta \mapsto 0$ and $\theta \mapsto \pi$, respectively. Figure 2 illustrates the second case, with the temperature coloring indicating the Dirac string along the negative p_z axis. Note that the $\mathcal{A}_u^{(1,2)}$ in Eq. (16) correspond to the gauge potentials chosen in the Wu-Yang construction for a magnetic monopole [137], up to global phases.

The curvature of Eq. (6) is explicitly evaluated for the eigenstates of Eq. (12) to be

$$\Omega_{u,i}^{(1,2)} = \mp \frac{p_i}{2p^3} = \Omega_{v,i}^{(1,2)}. \quad (17)$$

Hence, nonzero contributions with opposite signs arise at the origin of momentum space. Each of these has the form of a magnetic monopole, illustrated in Fig. 3. The temperature coloring reveals the increasing curvature approaching the origin, and the monopole is indicated by a black dot. Each monopole has strength $g = 1/2$, half that of the Wu-Yang monopole [137].

To determine the first Chern numbers associated with the monopoles, we integrate the curvature over a suitable closed surface containing the singularities according to Eq. (7). It is convenient to choose a 2-sphere $S_{p_0}^2$ of radius p and normal n around a point $p_0 \in \mathcal{P}_3$. Here, we pick the origin of momentum space such that $p_0 = 0$. Then,

$$\int_{S_{p_0}^2} d\Omega p^2 \Omega_u^{(1,2)} \cdot n = \mp 2\pi = \int_{S_{p_0}^2} d\Omega p^2 \Omega_v^{(1,2)} \cdot n, \quad (18)$$

where the unit normal n to the surface is pointing outwards. This reveals that the first Chern numbers are

$$N_u^{(1,2)} = N_v^{(1,2)} = \mp 1 \quad (\text{purely timelike case}). \quad (19)$$

The results (17) are independent of b_0 , since the eigenstates of Eq. (12) correspond to the Lorentz-invariant ones due to $[H_0, H_i] = 0$. In contrast, the dispersions (11) do depend on b_0 . The curvature characterizes the geometry of $P(U(1), \mathcal{P}_3)$ and hence is sensitive to the Weyl nodes at $p = 0$. However, it is insensitive to shifts of the nodes by $\pm b_0$ along the energy axis. Furthermore, as the curvature only detects topologically protected isolated points, the nodal surface $p = b_0$ plays no direct role.

Gauge transformations can be performed on the energy eigenstates such that $|u^{(1,2)}\rangle \mapsto |u^{(1,2)}\rangle' = \exp(i\phi)|u^{(1,2)}\rangle$ and $|v^{(1,2)}\rangle \mapsto |v^{(1,2)}\rangle' = \exp(i\phi)|v^{(1,2)}\rangle$. The resulting Berry connections are then given by

$$\mathcal{A}_{u'}^{(1)} = -\frac{1}{2p} \tan\left(\frac{\theta}{2}\right) \hat{\phi} = \mathcal{A}_{v'}^{(1)}, \quad (20a)$$

$$\mathcal{A}_{u'}^{(2)} = -\frac{1}{2p} \cot\left(\frac{\theta}{2}\right) \hat{\phi} = \mathcal{A}_{v'}^{(2)}. \quad (20b)$$

The gauge transformation preserves the Dirac strings while changing their location in momentum space: $\mathcal{A}_{u',v'}^{(1)}$

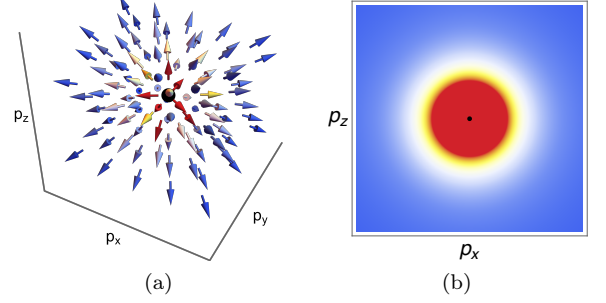


FIG. 3: (a) Vector field from a source of Berry curvature in Eq. (17), and (b) contour plot of its norm.

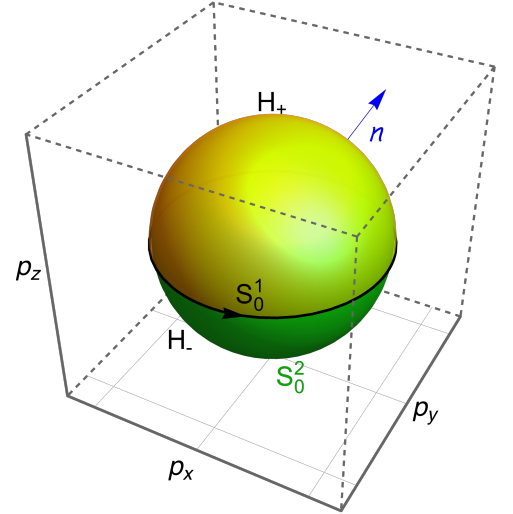


FIG. 4: 2-sphere S_0^2 around magnetic monopole with unit normal n and upper hemisphere H_+ bounded by the circle S_0^1 .

and $\mathcal{A}_{u',v'}^{(2)}$ have singularities for $\theta \mapsto \pi$ and $\theta \mapsto 0$, respectively.

Next, we determine the momentum-space geometric phase accumulated along a circle around the apex of a Weyl cone. Consider first a circle S_0^1 in the p_x - p_y plane, which is centered at $p_i = 0$ and is to be integrated in counterclockwise direction. Note that the Dirac strings of the eigenstates $|u^{(1)}\rangle$ and $|u^{(2)}\rangle$ are located at $p_z \in (0, \infty)$ and $p_z \in (-\infty, 0)$, respectively, such that $p_x = p_y = 0$, while the Dirac strings of $|v^{(1)}\rangle$ and $|v^{(2)}\rangle$ are at $p_z \in (0, \infty)$ and $p_z \in (-\infty, 0)$, respectively, with $p_x = p_y = 0$. So the Dirac strings lie outside S_0^1 , and the integrations can be carried out without issues. Using the Stokes theorem, the line integral of Eq. (5) can be reformulated as a surface integral over the curvature 2-

form Ω_ψ ,

$$\begin{aligned}\Phi &= \int_{H^+} d\Omega p^2 [\nabla_{\mathbf{p}} \times \mathcal{A}_\psi(\mathbf{p})] \cdot \mathbf{n} \\ &= \int_{H^+} d\Omega p^2 \Omega_\psi(-\mathbf{p}) \cdot \mathbf{n}.\end{aligned}\quad (21)$$

Note that H^+ corresponds to the upper hemisphere of S_0^2 such that $\partial H^+ = S_0^1$, as illustrated in Fig. 4. Hence, the surface that is integrated over is a subset of the surface considered in Eq. (18). The value of Φ in Eq. (21) corresponds to the Berry flux penetrating the surface H^+ .

Recall that the Stokes theorem is only applicable when neither H^+ nor ∂H^+ contain singularities. However, the former is clearly not the case for $|u^{(1)}\rangle$ and $|v^{(1)}\rangle$ due to their Dirac strings along the positive p_z axis. Thus, in this case we have to integrate along S_0^1 in clockwise direction, with the corresponding surface as the lower hemisphere H^- of S_0^2 . Based on Eq. (17), the opposite sign of the curvature $\Omega_{u,v}^{(1)}$ as compared to $\Omega_{u,v}^{(2)}$ comes into play, whereas the areas of H^\pm are equal. Therefore, performing either the line integrals along S_0^1 in the counterclockwise (clockwise) direction or the surface integral of Eq. (21) over H^+ (H^-) leads to the momentum-space geometric phases

$$\Phi_u^{(1)} = -\pi = \Phi_v^{(1)}, \quad \Phi_u^{(2)} = \pi = \Phi_v^{(2)}. \quad (22)$$

We can similarly determine the momentum-space geometric phases around a circle S_0^1 situated in the p_x - p_z plane, i.e., for $\phi = \pi/2$, as illustrated in Fig. 1b. This situation requires handling the Dirac strings along the p_z axis, using a gauge transformation to remove them. One possibility is to apply the following U(1) transformations on the u -type energy eigenstates of Eq. (12) with label $s = 1, 2$:

$$|u^{(s)}(p)\rangle \mapsto |u^{(s)}(p)\rangle' = \exp(i\chi^{(s)}) |u^{(s)}(p)\rangle, \quad (23a)$$

$$\chi^{(1)} = -\arctan \left[\cot(\phi) - \tan\left(\frac{\theta}{2}\right) \csc(\phi) \right], \quad (23b)$$

$$\chi^{(2)} = \phi + \arctan \left[\cot(\phi) + \tan\left(\frac{\theta}{2}\right) \csc(\phi) \right]. \quad (23c)$$

The v -type eigenstates of Eq. (12) should be gauge-transformed analogously. By doing so, the Dirac strings are moved to straight lines along the p_x axis, with those for $|u^{(1)}\rangle'$, $|v^{(1)}\rangle'$ aligned with $p_x \in (0, \infty)$, $p_y = p_z = 0$ and those for $|u^{(2)}\rangle'$, $|v^{(2)}\rangle'$ situated at $p_x \in (-\infty, 0)$, $p_y = p_z = 0$. The transformed situation is then analogous to the setting in the p_x - p_y plane considered previously, thereby reproducing the result (22).

B. Purely spacelike coefficient

We next consider the case of a purely spacelike coefficient b_μ , which incorporates spatial anisotropy. Without

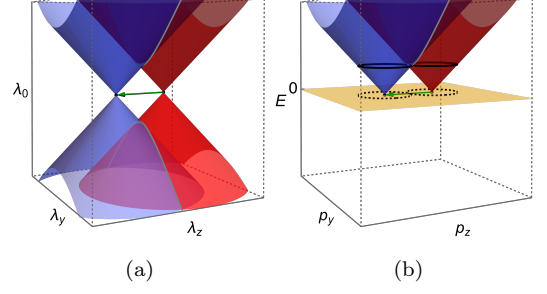


FIG. 5: Energy eigenvalues for the spacelike case (a) before and (b) after reinterpretation.

loss of generality, we can take $\delta = (0, 0, b_z)$ and $b_z > 0$. The hamiltonian then reads

$$H_\delta = H_0 + b_z \gamma^0 \gamma_5 \gamma^z, \quad (24)$$

with the standard Dirac hamiltonian H_0 of Eq. (9c). Note that $[H_0, H_\delta] \neq 0$, in contrast to the isotropic sector considered previously. The energy eigenvalues lie on Weyl cones shifted along the positive or negative p_z axis by b_z , as displayed in Fig. 5a. Applying the standard reinterpretation procedure generates two Weyl cones with apices on the $E = 0$ plane and with all other states having positive energy, as illustrated in Fig. 5b. This gives

$$E_u^{(1,2)} = |p \mp \delta|, \quad (25a)$$

$$E_v^{(1,2)} = |p \pm \delta|. \quad (25b)$$

After reinterpretation, the energy eigenstates as functions of cartesian momentum-space coordinates are readily obtained as

$$|u^{(1,2)}(p_i)\rangle = n_u^{(1,2)} \begin{pmatrix} \pm(p_x - ip_y) \\ E_u^{(1,2)} \mp p_z + b_z \\ -(p_x - ip_y) \\ \mp E_u^{(1,2)} + p_z \mp b_z \end{pmatrix}, \quad (26a)$$

$$|v^{(1,2)}(p_i)\rangle = n_v^{(1,2)} \begin{pmatrix} \pm(p_x - ip_y) \\ E_v^{(1,2)} \mp p_z - b_z \\ -(p_x - ip_y) \\ \mp E_v^{(1,2)} + p_z \pm b_z \end{pmatrix}, \quad (26b)$$

with the normalization factors

$$n_u^{(1,2)} = \frac{1}{2\sqrt{E_u^{(1,2)}(E_u^{(1,2)} \mp p_z + b_z)}}, \quad (27a)$$

$$n_v^{(1,2)} = \frac{1}{2\sqrt{E_v^{(1,2)}(E_v^{(1,2)} \mp p_z - b_z)}}. \quad (27b)$$

The Berry connections can be written in compact form

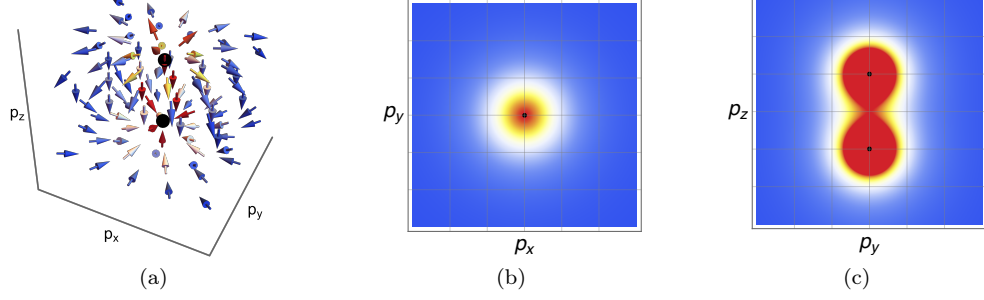


FIG. 6: (a) Vector-field plot of the curvature (29), (b) contour plot of its norm in the p_x - p_y plane, and (c) contour plot of its norm in the p_y - p_z plane.

using the modified dispersions (25),

$$\mathcal{A}_u^{(1,2)} = \frac{1}{2E_u^{(1,2)}(E_u^{(1,2)} \mp p_z + b_z)} \begin{pmatrix} -p_y \\ p_x \\ 0 \end{pmatrix}, \quad (28a)$$

$$\mathcal{A}_v^{(1,2)} = \frac{1}{2E_v^{(1,2)}(E_v^{(1,2)} \mp p_z - b_z)} \begin{pmatrix} -p_y \\ p_x \\ 0 \end{pmatrix}. \quad (28b)$$

The latter are analogous to the standard expressions of Eq. (16) when p_z is shifted by $\mp b_z$, where the Weyl nodes are situated. The curvatures are found from Eq. (6) to be

$$\Omega_{u,i}^{(1,2)} = \mp \frac{p_i \mp b_i}{2(E_u^{(1,2)})^3}, \quad (29a)$$

$$\Omega_{v,i}^{(1,2)} = \mp \frac{p_i \pm b_i}{2(E_v^{(1,2)})^3}. \quad (29b)$$

As in Eq. (17), these are magnetic-monopole analogues, but now shifted by $\pm b_z$ along the p_z axis. See Fig. 6a, where sink and source monopoles are represented by black dots. Note that significant Berry flux penetrates the plane through the origin and orthogonal to the line connecting the monopoles, as is visible in Fig. 6b.

Integrating over a 2-sphere S_0^2 around the origin of momentum space yields

$$\begin{aligned} \int_{S_0^2} d\Omega p^2 \Omega_u^{(1,2)} \cdot n &= \int_{S_0^2} d\Omega p^2 \Omega_v^{(1,2)} \cdot n \\ &= \mp 2\pi \Theta(p - b_z). \end{aligned} \quad (30)$$

The Heaviside step function $\Theta(x)$ ensures that nonzero contributions only arise when a singularity in the curvature is properly enclosed by the sphere. Analogously, integrations over spheres directly centered at the singularities provide

$$\int_{S_{\pm b}^2} d\Omega p^2 \Omega_u^{(1,2)} \cdot n = \mp 2\pi = \int_{S_{\pm b}^2} d\Omega p^2 \Omega_v^{(1,2)} \cdot n. \quad (31)$$

Contrary to the isotropic case of Sec. III A, the presence of the preferred direction δ in momentum space separates source and sink of the curvature from each other; see Fig. 6c. The behavior of the curvature along the line separating the monopoles bears similarities to the charge distribution of an electric dipole, where the distribution is constricted in the plane through the origin and orthogonal to the line.

We see that nonzero first Chern numbers

$$N_u^{(1,2)} = N_v^{(1,2)} = \mp 1 \quad (\text{purely spacelike case}) \quad (32)$$

are associated with any surface that encloses the points $p = \pm \delta$ where the Weyl nodes are situated. This indicates that the Weyl nodes are topologically protected and hence remain when a small fermion mass is introduced. In contrast, the curvature is insensitive to the degeneracies of the two Weyl cones at $p_z = 0$, indicated by grey lines in Fig. 5. Indeed, these degeneracies are not topologically protected and are lifted when a small fermion mass emerges.

Let $p_{\pm,i} := p_i \mp b_i$ be shifted momenta such that $p_{\pm,i} = 0$ at the Weyl nodes $p_i = \pm b_i$. We can adopt spherical coordinates $(p_{\pm}, \vartheta_{\pm}, \varphi_{\pm})$ with $p_{\pm} = |p_{\pm}|$ such that $p_{\pm,x} = p_x = p_{\pm} \sin \vartheta_{\pm} \cos \varphi_{\pm}$, $p_{\pm,y} = p_y = p_{\pm} \sin \vartheta_{\pm} \sin \varphi_{\pm}$, and $p_{\pm,z} = p_z \mp b_z = p_{\pm} \cos \vartheta_{\pm}$. Then, the energy eigenstates of Eq. (26) satisfy

$$|u^{(1)}(p_{+,i} + b_i)\rangle = \frac{\exp(-i\phi)}{\sqrt{2}} \begin{pmatrix} \xi^{(1)}(\vartheta_+, \varphi_+) \\ -\xi^{(1)}(\vartheta_+, \varphi_+) \end{pmatrix}, \quad (33a)$$

$$|v^{(2)}(p_{+,i} + b_i)\rangle = \frac{1}{\sqrt{2}} \begin{pmatrix} \xi^{(2)}(\vartheta_+, \varphi_+) \\ \xi^{(2)}(\vartheta_+, \varphi_+) \end{pmatrix}, \quad (33b)$$

$$|u^{(2)}(p_{-,i} - b_i)\rangle = \frac{1}{\sqrt{2}} \begin{pmatrix} \xi^{(2)}(\vartheta_-, \varphi_-) \\ \xi^{(2)}(\vartheta_-, \varphi_-) \end{pmatrix}, \quad (33c)$$

$$|v^{(1)}(p_{-,i} - b_i)\rangle = \frac{\exp(-i\phi)}{\sqrt{2}} \begin{pmatrix} \xi^{(1)}(\vartheta_-, \varphi_-) \\ -\xi^{(1)}(\vartheta_-, \varphi_-) \end{pmatrix}, \quad (33d)$$

with the two-component auxiliary spinors of Eq. (15) evaluated at the new angles ϑ_{\pm} and φ_{\pm} .

We can now calculate the momentum-space geometric phases by integrating along circles $S_{\pm b_i}^1$ in the p_x - p_y

plane centered at $p_i = \pm b_i$. The procedure of the purely timelike case is applicable with the Weyl nodes sitting at $p_{\pm,i} = 0$. In terms of the original momentum, the Dirac strings of the eigenstates $|u^{(1)}\rangle$ and $|u^{(2)}\rangle$ are located at $p_z \in (b_z, \infty)$ and $p_z \in (-\infty, -b_z)$, respectively, where $p_x = p_y = 0$. The Dirac strings of $|v^{(1)}\rangle$ and $|v^{(2)}\rangle$ run along $p_z \in (-b_z, \infty)$ and $p_z \in (-\infty, b_z)$, respectively, with $p_x = p_y = 0$. Therefore, the values of the momentum-space geometric phases are

$$\Phi_u^{(1)} = -\pi = \Phi_v^{(1)}, \quad \Phi_u^{(2)} = \pi = \Phi_v^{(2)}. \quad (34)$$

We can also compute the momentum-space geometric phase around the apices of the Weyl cones in the p_y - p_z plane, i.e., for $\varphi_+ = \varphi_- = \pi/2$. The Weyl cones are now separated along p_z in momentum space, an essential feature of this sector. As before, we apply a properly chosen $U(1)$ gauge transformation to the eigenstates. It is convenient to adapt Eq. (23) to the current setting, where the latter holds in the $p_{\pm,i}$ coordinates with the original Weyl nodes at $\mp b_z$ moved to $p_{\pm,i} = 0$. Expressing the spinors and the gauge transformation via the original momentum components p_i yields

$$|u^{(s)}(p)\rangle \mapsto |u^{(s)}(p)\rangle' = \exp(i\chi^{(s)})|u^{(s)}(p)\rangle, \quad (35a)$$

where the phases $\chi^{(s)}$ are given by

$$\chi^{(1)} = -\arctan \left[\cot(\varphi_-) - \tan\left(\frac{\vartheta_-}{2}\right) \csc(\varphi_-) \right], \quad (35b)$$

$$\chi^{(2)} = \varphi_+ + \arctan \left[\cot(\varphi_+) + \tan\left(\frac{\vartheta_+}{2}\right) \csc(\varphi_+) \right]. \quad (35c)$$

In an analogous manner, results for the v -type eigenstates are found. Here, the angles ϑ_{\pm} and φ_{\pm} must now be expressed in terms of p_i and b_z according to their definitions. As a result, the Dirac strings are relocated to straight lines parallel to the p_x axis. The Dirac strings for $|u^{(1)}\rangle'$, $|v^{(1)}\rangle'$ run along the sets $p_x \in (0, \infty)$, $p_y = 0$, and $p_z = \pm b_z$ and for $|u^{(2)}\rangle'$, $|v^{(2)}\rangle'$ we have $p_x \in (-\infty, 0)$, $p_y = 0$, and $p_z = \mp b_z$. This enables us to integrate along the circles in Fig. (5) in the p_y - p_z plane, which reproduces the momentum-space geometric phases of Eq. (34).

C. Generic spacelike coefficient

As a generalization of the purely spacelike sector, we consider the case of a spacelike b_μ with nonzero b_0 and b_z , with hamiltonian

$$H_b = H_0 - b_0 \gamma_5 + b_z \gamma^0 \gamma_5 \gamma^z, \quad (36)$$

and the reinterpreted dispersions

$$E_u^{(1,2)} = |p \mp b| \pm b_0, \quad (37a)$$

$$E_v^{(1,2)} = |p \pm b| \mp b_0. \quad (37b)$$

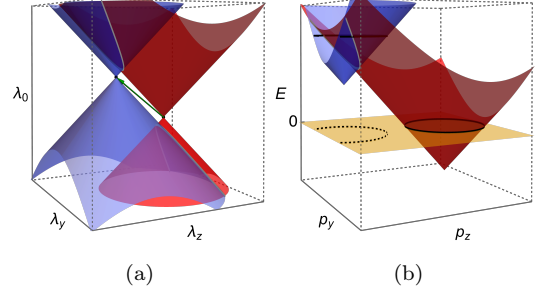


FIG. 7: Energy eigenvalues for the generic spacelike case (a) before and (b) after reinterpretation.

Now, the Weyl cones are shifted along the energy axis by $\pm b_0$ and along the p_z axis by $\pm b_z$. Both dispersions were discussed in detail in Ref. [24] and our solution of the concordance problem applies to the latter scenario. Note that $[H_b, H_6] = 0$ with H_6 of Eq. (24) for the purely spacelike case. Although the dispersions are different, the energy eigenstates for the purely spacelike sector quoted in Eq. (26) can be taken over without any modifications. Therefore, the curvatures (29) as well as the first Chern numbers (32) still hold.

In our recent paper [24] we were interested in the momentum-space geometric phases for the u - and v -type dispersions that intersect the Fermi plane. These are $E_u^{(2)}$ and $E_v^{(1)}$, represented by the red cone in Fig. 7b. As before, we integrate around circles $S_{\pm 6}^1$ lying in the p_x - p_z plane and encircling the apices of the corresponding Weyl cones. The shift of the cones along the energy axis caused by b_0 turns out to have no impact on the phases. By following the procedure of Sec. III B, we find

$$\Phi_u^{(2)} = \pi, \quad \Phi_v^{(1)} = -\pi. \quad (38)$$

This result can be verified numerically by integrating along small circles centered at the sites of a lattice covering the plane, as illustrated in Fig. 8. Nonzero contributions of $\Phi = \pm\pi$ arise for the circles on the red squares in the figure, which enclose the apices of the Weyl cones in \mathcal{D}_3 . In contrast, any circle without an apex inside contributes $\Phi = 0$. This method provides a numerical alternative for detecting the presence of Weyl nodes via the Berry connection.

The ground state of the theory with a generic spacelike b_μ has recently been studied using thermodynamic techniques and shown to be populated with fermions and antifermions of negative energies [24], unlike the vacuum in a Lorentz-invariant setting where no particles are present. This nontrivial ground state resembles that of electrons and holes in a one-particle description of certain Weyl semimetals [123]. The fermions and antifermions in the vacuum can be excited to positive-energy states via the exchange of energy with the thermodynamic bath. An excitation can acquire a momentum-space geometric phase if it traverses a loop enclosing the apex of the

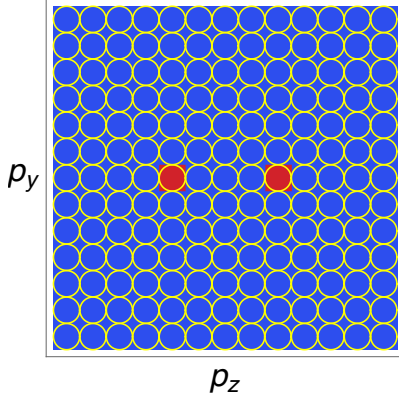


FIG. 8: Mesh of circles in the p_y - p_z plane.

corresponding Weyl cone, as indicated in Fig. 7b. The excitation can then drop back to the vacuum by releasing energy to the bath. The vacuum state itself therefore can acquire a nontrivial momentum-space geometric phase.

In the limit as the temperature T of the bath is taken to zero, the phase of the ground state freezes to a particular value Φ_0 . Since individual contributions to Φ_0 from each fermion or antifermion are quantized, Φ_0 itself is quantized. Moreover, the phase is topologically protected in this limit. We therefore can conclude that the vacuum in the theory with a generic spacelike b_μ can be chosen from among an infinite number of degenerate ground states, each characterized by a momentum-space geometric phase that is also topological. Investigating the possible phenomenological implications of this feature would be of definite interest but lies beyond our present scope.

IV. CPT-EVEN CASE

In this section, the momentum-space geometric phases associated with the action S_d of Eq. (2) are investigated. We examine in turn cases with isotropic, mixed, and spacelike $d_{\mu\nu}$ coefficients. The first Chern numbers are derived in each case, and the corresponding momentum-space geometric phases are then discussed.

A. Isotropic sector

The tracelessness of $d_{\mu\nu}$ implies a single isotropic combination of components exists. This isotropic combination can be written in diagonal matrix form as

$$d_{\mu\nu} = d_{00} \begin{pmatrix} 1 & 0 & 0 & 0 \\ 0 & \frac{1}{3} & 0 & 0 \\ 0 & 0 & \frac{1}{3} & 0 \\ 0 & 0 & 0 & \frac{1}{3} \end{pmatrix}. \quad (39)$$

The corresponding Lagrange density involves an additional time derivative, which leads to an unconven-

tional time evolution of asymptotic states. To restore conventional time evolution, the responsible terms can be removed from the Lagrange density via a suitable field redefinition. We follow the method presented in Ref. [138] and search for an invertible matrix A that satisfies $A^\dagger \gamma^0 \Gamma^0 A = \mathbb{1}_4$ with $\Gamma^0 = \gamma^0 + d^{\mu 0} \gamma_5 \gamma_\mu$, where $\mathbb{1}_n$ is the $(n \times n)$ identity matrix.

A possible choice for the matrix A is

$$A = \begin{pmatrix} C & \mathcal{B} \\ \mathcal{B} & C \end{pmatrix}, \quad C = A^+ \mathbb{1}_2, \quad \mathcal{B} = A^- \mathbb{1}_2, \quad (40a)$$

$$A^\pm = \sqrt{\frac{1 \pm \sqrt{1 - (d_{00})^2}}{2(1 - (d_{00})^2)}}, \quad (40b)$$

with inverse

$$A^{-1} = \sqrt{1 - (d_{00})^2} \begin{pmatrix} C & -\mathcal{B} \\ -\mathcal{B} & C \end{pmatrix}, \quad (41)$$

Note that this transformation is only valid for $d_{00} \in (-1, 1)$, as A becomes either singular or complex otherwise.

Let ψ be the Dirac field in the original SME action S_d . Then, a new Dirac field $\chi := A^{-1}\psi$ is introduced such that the latter satisfies a time-dependent Schrödinger-type equation $H_{\tilde{d}} \chi = i\partial_0 \chi$ with Hermitian hamiltonian

$$H_{\tilde{d}} = \gamma^0 \bar{A} (\gamma^j + d^{\mu j} \gamma_5 \gamma_\mu) \lambda^j A, \quad \bar{A} := \gamma^0 A^\dagger \gamma^0, \quad (42)$$

where \tilde{d} denotes the isotropic piece of $d_{\mu\nu}$ [62]. The time evolution of asymptotic states induced by the new hamiltonian is then conventional. The dispersions remain unaltered by the field redefinition

$$E_u^{(1,2)} = \frac{1 \mp d_{00}/3}{|1 \pm d_{00}|} p, \quad (43a)$$

$$E_v^{(1,2)} = \frac{1 \mp d_{00}/3}{|1 \pm d_{00}|} p. \quad (43b)$$

They describe two distinct Weyl cones with decreased and increased opening angle, respectively, as compared to the Lorentz-invariant case. See Figs. 9a and 9b for the case $d_{00} = 1/3$. Note that norms are computed only in the denominators. The dispersions have singularities at $d_{00} = \pm 1$, which are already excluded from the interval of validity of Eq. (40). Negative energies, which would occur for $d_{00} > 3$ or $d_{00} \leq -3$, are thereby also avoided.

The standard Dirac hamiltonian of Eq. (9c) commutes with the hamiltonian $H_{\tilde{d}}$ of Eq. (42) redefined by A . Hence, the energy eigenstates after the field redefinition are the standard ones of Eq. (12). Then, the Berry connection and curvature are unaffected by Lorentz violation, i.e., Eqs. (16) and (17) still hold. This implies the first Chern numbers

$$N_u^{(1,2)} = N_v^{(1,2)} = \mp 1 \quad (\text{isotropic case}). \quad (44)$$

B. Mixed sector d_{i0}

Next, we explore the mixed components d_{i0} with all others set to zero. Since d_{i0} are accompanied by an additional time derivative in the Lagrange density, we apply the method used in the isotropic case. The Dirac spinor field is to be transformed via a matrix A that obeys $A^\dagger \gamma^0 \Gamma^0 A = \mathbb{1}_4$ with $\Gamma^0 = \gamma^0 + d^{i0} \gamma_5 \gamma_i$. Via a generic *ansatz* based on the complete set of 16 matrices in spinor space, we can demonstrate that a suitable matrix A can be given by

$$A = \left(\begin{array}{c|c} \mathbb{1}_2 - \mathcal{D} & \varepsilon \\ \hline \varepsilon & \mathbb{1}_2 - \mathcal{D} \end{array} \right), \quad (45a)$$

$$\mathcal{D} = -\frac{\boldsymbol{\ell} \cdot \boldsymbol{\sigma}}{2(1 - \ell^2)}, \quad \varepsilon = \sqrt{3 - 4\ell^2} i \mathcal{D}, \quad (45b)$$

with inverse

$$A^{-1} = \frac{1}{1 - \ell^2} \left(\begin{array}{c|c} \tilde{\mathcal{D}} & \tilde{\varepsilon} \\ \hline \tilde{\varepsilon} & \tilde{\mathcal{D}} \end{array} \right), \quad (46a)$$

$$\tilde{\mathcal{D}} = \left(1 - \frac{3}{2} \ell^2 \right) \mathbb{1}_2 - \frac{1}{2} (1 - 2\ell^2) \boldsymbol{\ell} \cdot \boldsymbol{\sigma}, \quad (46b)$$

$$\tilde{\varepsilon} = -\frac{i}{2} \sqrt{3 - 4\ell^2} (\ell^2 \mathbb{1}_2 - \boldsymbol{\ell} \cdot \boldsymbol{\sigma}), \quad (46c)$$

conveniently expressed in terms of the Pauli matrices $\boldsymbol{\sigma} = (\sigma^x, \sigma^y, \sigma^z)$ and the form $\boldsymbol{\ell} := (d_{i0})$. The dispersions are readily obtained as

$$E_u^{(1,2)} = \frac{\pm \boldsymbol{\ell} \cdot \mathbf{p} + \Upsilon}{1 - \ell^2} = E_v^{(1,2)}, \quad (47a)$$

$$\Upsilon = \Upsilon(\mathbf{p}) = \sqrt{(1 - \ell^2) \mathbf{p}^2 + (\boldsymbol{\ell} \cdot \mathbf{p})^2}. \quad (47b)$$

Therefore, $\boldsymbol{\ell}$ tilts the Weyl cones and the presence of the factor $1 - \ell^2$ implies changes of their opening angles. Note that both Weyl cones are tilted in opposite directions, whereas the modified opening angle is the same for both cones. Figures 9c and 9d display these features for $d_{10} = d_{20} = 0$ and $d_{30} = 1/2$.

As in the isotropic case, a new Dirac spinor $\chi := A^{-1} \psi$ is defined such that the latter obeys a time-dependent Schrödinger-type equation $H_\ell \chi = i \partial_0 \chi$ with Hermitian hamiltonian

$$H_\ell = \gamma^0 \bar{A} \gamma^j \lambda^j A, \quad (48)$$

with the matrix \bar{A} defined according to Eq. (42). Now, the energy eigenstates for modified Dirac fermions are of the form

$$\begin{aligned} |u^{(1,2)}(\mathbf{p})\rangle &= |v^{(1,2)}(\mathbf{p})\rangle \\ &= n^{(1,2)} A^{-1} \begin{pmatrix} \pm(\bar{p}_x - i\bar{p}_y) \\ \Upsilon \mp \bar{p}_z \\ -(\bar{p}_x - i\bar{p}_y) \\ \mp \Upsilon + \bar{p}_z \end{pmatrix}, \end{aligned} \quad (49a)$$

with $\bar{p}_i := p_i - i(\boldsymbol{\ell} \times \mathbf{p})_i$, the inverse matrix A^{-1} given in Eq. (46), and the normalizations

$$\begin{aligned} n^{(1,2)} &= \frac{1}{2} \left(\Upsilon [\mp (1 - \ell^2) p_z \right. \\ &\quad \left. + (1 - d_{z0})(\Upsilon \mp \boldsymbol{\ell} \cdot \mathbf{p})] \right)^{-\frac{1}{2}}. \end{aligned} \quad (49b)$$

These equations permit us to compute the Berry connections. After some algebra, we find

$$\begin{aligned} \mathcal{A}_u^{(1,2)} &= \frac{1 - \ell^2}{2\Upsilon[(1 + d_{z0})(\Upsilon \mp \boldsymbol{\ell} \cdot \mathbf{p}) \mp (1 - \ell^2)p_z]} \\ &\times \begin{pmatrix} -p_y + (\boldsymbol{\ell} \times \mathbf{p})_x \\ p_x + (\boldsymbol{\ell} \times \mathbf{p})_y \\ (\boldsymbol{\ell} \times \mathbf{p})_z \end{pmatrix} = \mathcal{A}_v^{(1,2)}. \end{aligned} \quad (50)$$

The result incorporates a modification dependent on $\boldsymbol{\ell}$. The Dirac strings run along sets of points where the denominators of Eq. (50) vanish. These sets are intricate for nonzero $\boldsymbol{\ell}$.

The curvatures follow directly from Eq. (50). They read

$$\Omega_{u,i}^{(1,2)} = \mp \frac{(1 - \ell^2) p_i}{2\Upsilon^3(\mathbf{p})} = \Omega_{v,i}^{(1,2)}. \quad (51)$$

Note that these expressions reduce as required to the standard results (16) and (17), respectively, for $d_{i0} \rightarrow 0$. Note also that the curvatures are unaffected by Lorentz violation at the linear level. Moreover, as in the Lorentz-invariant case, $\Omega_{u,i}^{(1)} + \Omega_{u,i}^{(2)} = 0 = \Omega_{v,i}^{(1)} + \Omega_{v,i}^{(2)}$. The singularities are situated at $p_i = 0$ and the first Chern numbers can be computed in spherical coordinates, yielding the results

$$N_u^{(1,2)} = N_v^{(1,2)} = \mp 1 \quad (\text{first mixed case}). \quad (52)$$

C. Mixed sector d_{0i}

This section concerns the mixed coefficients d_{0i} , with all others set to zero. It is helpful to introduce the three-component form $\tilde{\boldsymbol{\ell}} := (d_{0i})$. Unlike the previous isotropic and mixed configurations of Secs. IV A and IV B, respectively, the coefficients d_{0i} are not contracted with an additional time derivative. It is therefore unnecessary to redefine the Dirac spinor field. The hamiltonian reads

$$H_{\tilde{\boldsymbol{\ell}}} = H_0 + d_{0i} \gamma^0 \gamma_5 \gamma^i \lambda_i, \quad (53)$$

where H_0 is the Dirac hamiltonian of Eq. (9c). The dispersions are

$$E_u^{(1,2)} = \pm \tilde{\boldsymbol{\ell}} \cdot \mathbf{p} + p = E_v^{(1,2)}. \quad (54)$$

This reveals that $\tilde{\boldsymbol{\ell}}$ tilts the Weyl cones, while preserving their opening angles. See Figs. 9e and 9f for the case $d_{01} = d_{02} = 0$ and $d_{03} = 1/2$.

The vanishing commutator $[H_0, H_j] = 0$ implies that the eigenstates of the Dirac hamiltonian remain unaffected by the coefficients d_{0i} , i.e., they can be taken over from Eq. (12). The curvature therefore takes the same form as in Eq. (17). The tilting of the Weyl cones has no effect, so the integrated curvatures are given by Eq. (18). We thus obtain the first Chern numbers as

$$N_u^{(1,2)} = N_v^{(1,2)} = \mp 1 \quad (\text{second mixed case}). \quad (55)$$

D. Purely spacelike off-diagonal coefficients d_{ij}

Finally, we explore the case of purely spacelike d coefficients such that $d_{00} = d_{i0} = d_{0j} = 0$ and $d_{ij} \neq 0$ for $j > i$. No additional time derivative appears, and the hamiltonian is

$$H_d = H_0 + d_{ij}\gamma^0\gamma_5\gamma^i\lambda_j, \quad (56)$$

where H_0 is the Dirac hamiltonian of Eq. (9c).

It is convenient to define the matrices $\mathbb{D}^{(\pm)}$ with components $(\mathbb{D}^{(\pm)})_{ij} := \delta_{ij} \pm d_{ij}$. Then, the exact dispersions can be cast into the compact form

$$E_u^{(1,2)} = |\mathbb{D}^{(\mp)}\mathbf{p}| = E_v^{(1,2)}. \quad (57)$$

The two Weyl cones are spatially distorted such that they exhibit several intersections with each other. See Figs. 9g and 9h for the case $d_{12} = d_{13} = d_{23} = 3/4$. The u - and reinterpreted v -type spinor-valued energy eigenstates are

$$\begin{aligned} |u^{(1,2)}(\mathbf{p})\rangle &= n_u^{(1,2)} \begin{pmatrix} \pm E_u^{(1,2)} + p_z \\ (\mathbb{D}^{(\mp)}\mathbf{p})_x + i(\mathbb{D}^{(\mp)}\mathbf{p})_y \\ -E_u^{(1,2)} \mp p_z \\ \mp(\mathbb{D}^{(\mp)}\mathbf{p})_x \mp i(\mathbb{D}^{(\mp)}\mathbf{p})_y \end{pmatrix} \\ &= |v^{(1,2)}(\mathbf{p})\rangle, \end{aligned} \quad (58a)$$

with the normalization factors

$$n_u^{(1,2)} = \frac{1}{2\sqrt{E_u^{(1,2)}(E_u^{(1,2)} \pm p_z)}}. \quad (58b)$$

The Berry connection has an intricate form, but it can be expressed in a compact manner as follows:

$$\mathcal{A}_u^{(1,2)} = \frac{\mathbf{p} \times \boldsymbol{\zeta}^{(1,2)}}{2E_u^{(1,2)}(E_u^{(1,2)} \pm p_z)} = \mathcal{A}_v^{(1,2)}, \quad (59a)$$

with the auxiliary vectors

$$\boldsymbol{\zeta}^{(1,2)} := \begin{pmatrix} \pm d_{13} + d_{12}d_{23} \\ \pm d_{23} \\ 1 \end{pmatrix}. \quad (59b)$$

The Dirac strings run along sets where $E_u^{(1,2)} = \mp p_z$. These connections reduce to Eq. (16) for $d_{ij} = 0$, modulo global signs and an interchange of the labels $(1, 2)$.

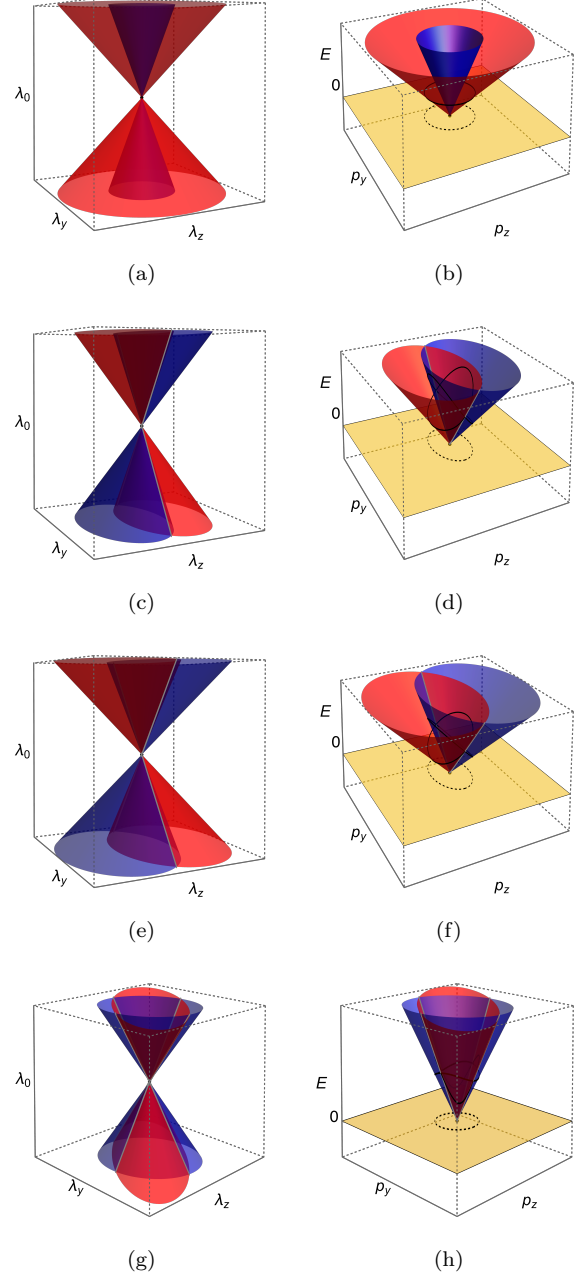


FIG. 9: Energy eigenvalues before and after reinterpretation for (a), (b) the isotropic case (43), (c), (d) the first mixed case (47), (e), (f) the second mixed case (54), and (g), (h) the purely spacelike case (57).

The curvatures take forms analogous to the standard ones of Eq. (17), but with p in the denominators replaced by the modified dispersion with the appropriate label,

$$\Omega_{u,i}^{(1,2)} = \mp \frac{p_i}{2(E_u^{(1,2)})^3} = \Omega_{v,i}^{(1,2)}. \quad (60)$$

The signs appearing in Eq. (60) and the interchange of labels can be understood by applying a parity transfor-

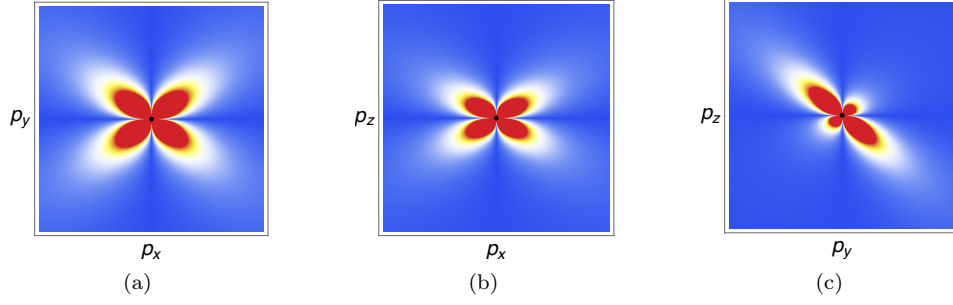


FIG. 10: Contour plot of the curvature (60) (a) in the p_x - p_y plane, (b) in the p_x - p_z plane, and (c) in the p_y - p_z plane.

mation in momentum space, $p \mapsto -p$. This adapts the labeling and global signs of Eq. (59) for $d_{ij} = 0$ to the ones of Eq. (16). The sign change of the curvature under $p \mapsto -p$ is compensated by the additional sign change $\nabla_{\mathbf{p}} \mapsto -\nabla_{\mathbf{p}}$.

The sums of $\Omega_{u,i}^{(1,2)}$ and $\Omega_{v,i}^{(1,2)}$ produce nonzero results, unlike the case of nonzero d_{i0} discussed in Sec. IV B. To display these modifications, contour plots of the norms $|(\Omega_{u,i}^{(1)} + (\Omega_{u,i}^{(2)}))|$ in three mutually orthogonal planes are presented in Fig. 10 for the nonzero values $d_{12} = d_{13} = d_{23} = 3/4$ of the three off-diagonal spatial d -type coefficients. In two planes the curvature has a symmetrical butterfly shape, but in the third the butterfly shape is distorted. These plots are reminiscent of quadrupole distributions.

Due to the involved form of the dispersions, it is challenging to integrate the curvature analytically. However, numerical computations can be performed to reveal that the first Chern numbers are

$$N_u^{(1,2)} = N_v^{(1,2)} = \mp 1 \quad (\text{spacelike case}). \quad (61)$$

E. Momentum-space geometric phases

We can determine the momentum-space geometric phases for the various scenarios with nonzero coefficients $d_{\mu\nu}$ along circles in \mathcal{P}_3 . However, unlike the b_μ sector, the $d_{\mu\nu}$ coefficients do not separate the Weyl cones along a direction in \mathcal{P}_4 . Instead, each Weyl cone is deformed differently, which also lifts the fourfold degeneracy. Projecting the circles in \mathcal{P}_3 onto these cones implies closed loops, but E varies along these curves.

For the isotropic case of Sec. IV A and the second mixed sector of Sec. IV C, the curvatures match those of Eq. (17). Integrating the latter around apices of the Weyl cones along circles in \mathcal{P}_3 and avoiding the Dirac strings according to the procedure of Sec. III A yields the momentum-space geometric phases

$$\Phi_u^{(1)} = -\pi = \Phi_v^{(1)}, \quad \Phi_u^{(2)} = \pi = \Phi_v^{(2)}. \quad (62)$$

This result is in agreement with Eq. (22) even though the loops on the Weyl cones in \mathcal{P}_4 are no longer circles

of constant energy. The projections of these loops are shown in Figs. 9b and 9f.

For the first mixed sector of Sec. IV B and the purely spacelike regime of Sec. IV D, the curvatures are modified by the Lorentz violation. The calculations of the integrals to obtain the momentum-space geometric phases therefore differ from those of the conventional Dirac theory. However, performing the computations explicitly reveals that the momentum-space geometric phases for these sectors are again given by Eq. (62) modulo 2π .

V. ALTERNATIVE INVARIANTS

Our treatment of topological properties above is based on the first Chern number. This section presents some results on alternative topological invariants.

The gap nodes at the Fermi energy $E_F = 0$, known as Fermi points, can be characterized by the topological invariant [139, 140]

$$N_a = \text{tr} \oint_{\Sigma_a} dn^\sigma n_\sigma, \quad (63a)$$

$$n_\sigma = \frac{1}{24\pi^2} \varepsilon_{\mu\nu\rho\sigma} S \frac{\partial \mathcal{D}}{\partial p_\mu} S \frac{\partial \mathcal{D}}{\partial p_\nu} S \frac{\partial \mathcal{D}}{\partial p_\rho}. \quad (63b)$$

Here, $dn^\sigma = d\Sigma_a n^\sigma$ is the volume element of the closed three-dimensional hypersurface Σ_a with unit 4-vector normal n^σ . Also, $\mathcal{D} = \mathcal{D}(i\lambda_4, \lambda_k)$ is the Dirac operator in momentum space and $S = \mathcal{D}^{-1}(i\lambda_4, \lambda_k)$ the Dirac propagator, both being evaluated at imaginary energies $\lambda_0 = i\lambda_4$ via a Wick rotation. The trace is computed over spinor indices, and $\varepsilon_{\mu\nu\rho\sigma}$ is the totally antisymmetric Levi-Civita symbol.

The topological invariant N_a takes integer values, $N_a \in \mathbb{Z}$, and is sensitive to isolated Fermi points. For $N_a = 0$, the topology of the Fermi point is trivial. When $N_a \neq 0$, the topology of the bundle $P(U(1), \mathcal{P}_4)$ is nontrivial and the Fermi points are insensitive to small perturbations.

Note that N_a is evaluated in the energy-momentum space \mathcal{P}_4 with $(\lambda_0, \lambda_k) \in \mathcal{P}_4$. In contrast, both the Berry curvature and the momentum-space geometric phases considered above are evaluated in \mathcal{P}_3 . Also, Eq. (63)

offers a computational advantage in that it requires only the propagator in the Dirac sector of the SME. In particular, knowledge of the eigenstates of the quantum system is unnecessary.

A. CPT-odd case

The Dirac propagator for each one of the coefficients of the SME fermion sector is known [65, 127]. In particular, for the b_μ sector with a vanishing fermion mass, we cast the result into

$$S_b(\lambda_0, \lambda_k) = \frac{1}{\Delta} (\xi_\mu \gamma^\mu + \zeta_\mu \gamma_5 \gamma^\mu), \quad (64a)$$

$$\xi^\mu = (\lambda^2 + b^2) \lambda^\mu - 2(b \cdot \lambda) b^\mu, \quad (64b)$$

$$\zeta^\mu = -2(b \cdot \lambda) \lambda^\mu + (\lambda^2 + b^2) b^\mu, \quad (64c)$$

$$\Delta = (\lambda - b)^2 (\lambda + b)^2. \quad (64d)$$

The trace of the matrix density $\mathcal{N}_\sigma n^\sigma$ of Eq. (63) can be evaluated in covariant form,

$$\begin{aligned} \text{tr}(\mathcal{N}_\sigma n^\sigma) &= \frac{1}{\pi^2 \Delta^2} \tilde{\eta}_{\mu\nu} n^\mu \left\{ 4\lambda^\nu (b \cdot \lambda) (\lambda^2 + b^2) \right. \\ &\quad \left. - b^\nu [4(b \cdot \lambda)^2 + (\lambda^2 + b^2)^2] \right\} \Big|_{\lambda_0 \rightarrow i\lambda_4}, \end{aligned} \quad (65)$$

with $\tilde{\eta}_{\mu\nu} := \text{diag}(i, -1, -1, -1)$ and the Minkowski metric $\eta_{\mu\nu}$ is employed for all remaining scalar products.

First, let us evaluate N_a for a purely timelike b_μ . The hypersurface Σ_a is chosen as a 3-sphere parametrized as

$$\begin{pmatrix} \lambda_4 \\ \lambda_x \\ \lambda_y \\ \lambda_z \end{pmatrix} = \lambda \begin{pmatrix} \sin \theta \sin \phi \sin \chi \\ \sin \theta \sin \phi \cos \chi \\ \sin \theta \cos \phi \\ \cos \theta \end{pmatrix}, \quad (66)$$

with $\lambda := \sqrt{\sum_i \lambda_i^2}$ and angles $\theta \in [0, \pi]$, $\phi \in [0, \pi]$, and $\chi \in [0, 2\pi]$. Integrations around the Weyl nodes at $\lambda_4 = \pm i b_0$ provide $N_a = \mp 1$. To avoid singularities of the integrand, it is important to choose the radius of Σ_a small enough such that the nodal circle of Fig. 1a is not contained in it. Similarly, we can consider a purely space-like b_μ with $\mathbf{b} = (0, 0, b_z)$, where integrations around the Weyl nodes $(\lambda_k) = \pm \mathbf{b}$ result in $N_a = \pm 1$, as well. Thus, we conclude that these points are topologically protected, which agrees with the results related to the curvatures of Eqs. (18), (30), and (31). An integration over a 3-sphere around the origin $\lambda_k = 0$ without enclosing one of the Weyl nodes leads to $N_a = 0$, as expected.

The nodal circle of the isotropic b_μ sector, which is visible in Fig. 1a, represents a Fermi surface that corresponds to a 2-sphere with one of the spatial momentum components disregarded. The topological properties of this contour must be determined differently from those

of isolated Weyl or Dirac points. Here, integration must be performed along a closed curve γ that encircles the nodal line. For a modified Dirac theory with Dirac operator \mathcal{D} and propagator S_F , the corresponding topological invariant is [140]

$$N_1 = \text{tr} \oint_\gamma \frac{d\vartheta}{2\pi i} S(\lambda_4, \lambda_k) \partial_\vartheta \mathcal{D}(\lambda_4, \lambda_k), \quad (67)$$

with the trace performed over the spinor indices. The curve γ is chosen as a loop parametrized in terms of the angle $\vartheta \in [0, 2\pi]$ and shifted appropriately such that it runs around the nodal circle. In particular, $\lambda_4 = -\sin(\vartheta)$, where we choose $\lambda_x = 0$, $\lambda_y = \cos \varphi (\cos \vartheta + b_0)$, and $\lambda_z = \sin \varphi (\cos \vartheta + b_0)$. Then, the nodal circle in the λ_y - λ_z plane is enclosed by a loop centered at the point $\lambda_4 = 0$, $\lambda_y = b_0 \cos \varphi$, and $\lambda_z = b_0 \sin \varphi$ and orthogonal to the tangent vector of the nodal circle at this point.

Applying Eq. (67) with Eq. (64) inserted and $\lambda_0 \mapsto i\lambda_4$, we obtain that $N_1 = 0$. This holds because the propagator for the b_μ model, stated in Eq. (64), involves the overall factor Δ^{-1} , given by Eq. (64d). For the isotropic sector, Δ^{-1} is a product of scalar toy model propagators of the form

$$G_\pm(\lambda_4, \lambda_k) = \frac{1}{(i\lambda_4 \pm \lambda_F)^2 - \lambda^2}, \quad (68)$$

with $\lambda_0 \mapsto i\lambda_4$ and λ_F interpreted as the Fermi momentum. The latter have Fermi surfaces at $\lambda_4 = 0$, $\lambda = \lambda_F$. Integration along a circle around $\lambda_x = \lambda_F$ implies $N_1^\pm = \mp 1$. Since the Fermi surfaces with $N_1^\pm = \mp 1$ are encircled simultaneously when the integral of Eq. (67) is evaluated for Eq. (64), the nontrivial topological quantum numbers compensate each other: $N_+ + N_- = -1 + 1 = 0$. This means that the Fermi surface for the purely timelike sector of the b_μ model is topologically trivial, i.e., it is not protected against small perturbations. Indeed, introducing a small fermion mass opens a gap and the Fermi surface vanishes, confirming the computational outcome.

B. CPT-even case

The propagator of the $d_{\mu\nu}$ sector has a form analogous to Eq. (64) for the b_μ coefficients [65, 127]. However, the dependence on the four-momentum is more involved,

$$S_d(\lambda_0, \lambda_k) = \frac{1}{\Delta} (\xi_\mu \gamma^\mu + \zeta_\mu \gamma_5 \gamma^\mu), \quad (69a)$$

$$\xi^\mu = [\lambda^2 + (d \cdot \lambda)^2] \lambda^\mu - 2(\lambda \cdot d \cdot \lambda) d^{\mu\nu} \lambda_\nu, \quad (69b)$$

$$\zeta^\mu = 2(\lambda \cdot d \cdot \lambda) \lambda^\mu - [\lambda^2 + (d \cdot \lambda)^2] d^{\mu\nu} \lambda_\nu, \quad (69c)$$

$$\Delta = (\lambda + d \cdot \lambda)^2 (\lambda - d \cdot \lambda)^2, \quad (69d)$$

where $d \cdot \lambda$ denotes $d^{\mu\nu} \lambda_\nu$.

Using the above propagator, we seek to evaluate the integral for the topological quantum number N_a of Eq. (63) for each of the cases discussed in Secs. IV A – IV D. The integrals are challenging to carry out for generic coefficients, so we perform computations for specific values. Note that the integration may be problematic when some SME coefficients become large. For example, for $d_{i0} = -0.58$, the dispersion of Eq. (47) becomes complex in certain regions of momentum space, which renders the value of Eq. (63) invalid as a topological charge. Similarly, for $d_{0i} = -0.58$ the dispersion of Eq. (54) is zero in particular regions, whereupon Eq. (63) becomes singular. However, no such issues occur for the purely spacelike coefficients d_{ij} with $i \neq j$ because $\lambda_i (\mathbb{D}^{(\pm)T})_{ik} (\mathbb{D}^{(\pm)})_{kj} \lambda_j > 0$ for $\lambda_k \neq 0$, which prevents complex or zero values of the dispersions of Eq. (57) from occurring beyond the Weyl nodes.

For the isotropic case, computation yields the results

$$N_a = \begin{cases} 0 & 0 \leq |d_{00}| < 1, \\ \pm 1 & d_{00} = \mp 1, \\ \pm 2 & d_{00} \in (\mp 1, \mp 3), \\ \pm 1 & d_{00} = \mp 3, \\ 0 & |d_{00}| > 3. \end{cases} \quad (70)$$

This indicates a trivial topology for d_{00} lying in a finite, open interval centered around the Lorentz-invariant case. At $|d_{00}| = 1$ the dispersion (43) becomes singular, which is reflected in the apparent topology change. Note also that the form (40) of the matrix A , which was introduced to remove the additional time derivative from the Lagrange density appearing in this sector, is inapplicable for $|d_{00}| > 1$. Another topology change is seen to occur at $|d_{00}| = 3$, where one of the two dispersions of Eq. (43) vanishes. The corresponding fermion mode thus cannot provide any contribution to N_a , which reduces it by one unit to $|N_a| = 1$.

For the mixed coefficients d_{i0} , d_{0i} and the purely spacelike ones d_{ij} , we obtain $N_a = 0$ for values within a range around zero. Each of these sectors can thus be interpreted as topologically trivial. This result follows because the Weyl nodes are joined, and the opposite topological charges of the individual nodes therefore cancel each other.

VI. SUMMARY AND OUTLOOK

This work concerns the effect of a background on the momentum-space geometric phases associated with the relativistic motion of massless spin- $\frac{1}{2}$ Weyl fermions in Lorentz-violating models, where the role of the background is played by the coefficients for Lorentz violation. Two examples are studied. Section III discusses the scenario with CPT violation involving a coefficient b_μ , while Sec. IV considers the CPT-preserving case with a coefficient $d_{\mu\nu}$. The topological properties of the momentum-space geometric phases are investigated using the Berry

curvature and the first Chern number. Alternative topological invariants are explored in Sec. V.

When a nonzero coefficient b_μ is present, our results demonstrate that significant changes occur to the Berry curvature when the two Weyl cones become nondegenerate along a spatial direction in momentum space. Then, the source and sink of the curvature, which coincide in the Lorentz-invariant regime, are separated and a Berry flux emerges in the plane orthogonal to the line of separation. Momentum-space geometric phases of $\pm\pi$ can accumulate when the apices of the Weyl cones are encircled during the fermion motion. These geometric phases play a special role for occupied fermion and antifermion states at $E = 0$, which are of particular relevance in certain scenarios with large Lorentz violation.

In the presence of a nonzero $d_{\mu\nu}$ coefficient, the Weyl cones remain joined in momentum space, but they can be subject to tilts or spatial distortions. Our results demonstrate that a tilt leaves unaffected the Berry curvature, whereas spatial distortions of Weyl cones are reflected in curvature distortions. The norm of the total curvature for u - and v -type spinors no longer vanishes, and lines of constant curvature acquire a butterfly shape. The topological charges of the Weyl nodes remain ± 1 . Momentum-space geometric phases of $\pm\pi$ emerge along loops encircling the apices of Weyl cones.

Our investigations reveal that the geometry of the $U(1)$ bundle of energy eigenstates over momentum space remains unaffected when the Weyl cones are shifted along the energy axis, when they are tilted, or when their opening angle changes. However, a separation of the Weyl cones along a spatial-momentum direction and spatial deformations both impact the geometry. These results are consistent with our studies of certain topological invariants other than the first Chern number, which confirm that topological charges are present at degenerate points in energy-momentum space. These invariants are determined based on the propagator of a theory, rather than the hamiltonian and its eigenstates.

The results in this work represent an initial step toward the establishment of a comprehensive treatment of momentum-space geometric phases in the full SME. Several direct theoretical extensions of our analysis can be envisaged for future work. An immediate possibility of definite interest is the extension of the results to other coefficients in the fermion sector, including nonminimal ones. Applications of these ideas to other sectors of the SME are also of prospective interest.

Another area for exploration is associated with lifting the assumption of time-independent and spatially homogeneous coefficients. In practical applications to fundamental physics, the cartesian coefficients for Lorentz violation are typically assumed to be constant in a canonical Sun-centered frame [141–143], which provides an approximately inertial reference frame over applicable experimental timescales. However, experimental measurements are performed in a noninertial frame on or near the Earth's surface, which implies time-dependent variations

in the observable coefficients for Lorentz violation [144]. These variations oscillate at harmonics of the Earth's sidereal frequency and hence are adiabatic on typical experimental timescales. A theoretical treatment of the implications of these oscillations for observable geometric phases would be of definite interest.

Applications in the context of condensed-matter physics also have worthwhile prospects. Consider, for example, a b_μ -type Weyl semimetal of finite volume, in which one or more spatial components of b_μ are nonzero within a certain spatial domain D but vanish outside D . On the boundary ∂D , the topology of the ground state changes from nontrivial to trivial, implying the existence of interesting surface states such as Fermi arcs or drum-head surface states. A nontrivial ground-state topology may also modify measurable transport properties.

Other novel experimental applications of our work may also be feasible. In the presence of Lorentz violation, the value of the momentum-space geometric phase is fixed for each nondegenerate Weyl cone. Also, when the Weyl cones are separated or distorted along spatial-momentum directions, the total Berry curvature differs from the zero value of the Lorentz-invariant case. These properties

therefore establish the momentum-space geometric phase and the Berry curvature as gauge-invariant observables for Lorentz violation. The experimental search for spin-nondegenerate Lorentz violation governed by b_μ and $d_{\mu\nu}$ can thus be reinterpreted as the search for fixed values of the momentum-space geometric phases of massless spin- $\frac{1}{2}$ fermions. In particular, even infinitesimal background coefficients suffice to generate a nontrivial effect, so the detection of Lorentz violation via momentum-space geometric phases is unhampered by experimental sensitivity to the size of the coefficients. Adapting this result to implementing a realistic experimental scenario for a magnitude-independent detection of Lorentz violation is an open challenge of considerable prospective interest.

ACKNOWLEDGMENTS

This work is supported in part by the U.S. Department of Energy under grant DE-SC0010120, by grants FAPEMA Universal 00830/19 and CNPq Produtividade 310076/2021-8, by CAPES/Finance Code 001, and by the Indiana University Center for Spacetime Symmetries.

-
- [1] S. Pancharatnam, Generalized theory of interference, and its applications, *Proc. Indian Acad. Sci. A* **44**, 247 (1956).
 - [2] M. V. Berry, Quantal phase factors accompanying adiabatic changes, *Proc. Roy. Soc. Lond. A* **392**, 45 (1984).
 - [3] B. Simon, Holonomy, the quantum adiabatic theorem, and Berry's phase, *Phys. Rev. Lett.* **51**, 2167 (1983).
 - [4] Y. Aharonov and J. Anandan, Phase change during a cyclic quantum evolution, *Phys. Rev. Lett.* **58**, 1593 (1987).
 - [5] J. Zak, Berry's phase for energy bands in solids, *Phys. Rev. Lett.* **62**, 2747 (1989).
 - [6] D. Chruściński and A. Jamiolkowski, *Geometric Phases in Classical and Quantum Mechanics* (Birkhäuser Boston (MA), USA, 2004).
 - [7] M. Nakahara, *Geometry, Topology and Physics* (Institute of Physics Publishing, Bristol and Philadelphia, 2003).
 - [8] D. Vanderbilt, *Berry Phases in Electronic Structure Theory, Electric Polarization, Orbital Magnetization and Topological Insulators* (Cambridge University Press, Cambridge, UK, 2018).
 - [9] V. A. Kostelecký and S. Samuel, Spontaneous breaking of Lorentz symmetry in string theory, *Phys. Rev. D* **39**, 683 (1989).
 - [10] V. A. Kostelecký and R. Potting, CPT and strings, *Nucl. Phys. B* **359**, 545 (1991).
 - [11] S. Weinberg, Effective field theory, past and future, *PoS CD09*, 001 (2009), arXiv:0908.1964 [hep-th].
 - [12] V. A. Kostelecký and R. Potting, CPT, strings, and meson factories, *Phys. Rev. D* **51**, 3923 (1995), arXiv:hep-ph/9501341.
 - [13] D. Colladay and V. A. Kostelecký, CPT violation and the standard model, *Phys. Rev. D* **55**, 6760 (1997), arXiv:hep-ph/9703464.
 - [14] D. Colladay and V. A. Kostelecký, Lorentz-violating extension of the standard model, *Phys. Rev. D* **58**, 116002 (1998), arXiv:hep-ph/9809521.
 - [15] V. A. Kostelecký, Gravity, Lorentz violation, and the standard model, *Phys. Rev. D* **69**, 105009 (2004), arXiv:hep-th/0312310.
 - [16] V. A. Kostelecký and Z. Li, Backgrounds in gravitational effective field theory, *Phys. Rev. D* **103**, 024059 (2021), arXiv:2008.12206 [gr-qc].
 - [17] B. Q. Lv *et al.*, Experimental discovery of Weyl semimetal TaAs, *Phys. Rev. X* **5**, 031013 (2015), arXiv:1502.04684 [cond-mat.mtrl-sci].
 - [18] A. Tamai, Q. S. Wu, I. Cucchi, F. Y. Bruno, S. Riccò, T. K. Kim, M. Hoesch, C. Barretero, E. Giannini, C. Besnard, A. A. Soluyanov, and F. Baumberger, Fermi arcs and their topological character in the candidate type-II Weyl semimetal MoTe₂, *Phys. Rev. X* **6**, 031021 (2016).
 - [19] B. Yan and C. Felser, Topological materials: Weyl semimetals, *Ann. Rev. Condensed Matter Phys.* **8**, 337 (2017), arXiv:1611.04182 [cond-mat.mtrl-sci].
 - [20] N. P. Armitage, E. J. Mele, and A. Vishwanath, Weyl and Dirac semimetals in three-dimensional solids, *Rev. Mod. Phys.* **90**, 015001 (2018), arXiv:1705.01111 [cond-mat.str-el].
 - [21] H. Gao, J. W. F. Venderbos, Y. Kim, and A. M. Rappe, Topological semimetals from first principles, *Annu. Rev. Mat. Res.* **49**, 153 (2019).
 - [22] V. A. Kostelecký, R. Lehnert, N. McGinnis, M. Schreck, and B. Seradjeh, Lorentz violation in Dirac and Weyl semimetals, *Phys. Rev. Res.* **4**, 023106 (2022), arXiv:2112.14293 [cond-mat.mes-hall].

- [23] A. Gómez, R. M. von Dossow, A. Martín-Ruiz, and L. F. Urrutia, Lorentz invariance violation and the CPT-odd electromagnetic response of a tilted anisotropic Weyl semimetal, *Phys. Rev. D* **109**, 065005 (2024), arXiv:2312.07791 [hep-th].
- [24] V. A. Kostelecký, R. Lehnert, M. Schreck, and B. Seradjeh, Physical interpretation of large Lorentz violation via Weyl semimetals, *New J. Phys.* **27**, 073901 (2025), arXiv:2412.18034 [hep-ph].
- [25] V. A. Kostelecký, R. Lehnert, M. Schreck, and B. Seradjeh, Nonperturbative Lorentz violation and field quantization, *Phys. Lett. B* **865**, 139414 (2025), arXiv:2412.19733 [hep-th].
- [26] V. A. Kostelecký and R. Lehnert, Stability, causality, and Lorentz and CPT violation, *Phys. Rev. D* **63**, 065008 (2001), arXiv:hep-th/0012060.
- [27] A. G. Grushin, Consequences of a condensed matter realization of Lorentz-violating QED in Weyl semi-metals, *Phys. Rev. D* **86**, 045001 (2012), arXiv:1205.3722 [hep-th].
- [28] J. Behrends, S. Roy, M. H. Kolodrubetz, J. H. Bardarson, and A. G. Grushin, Landau levels, Bardeen polynomials, and Fermi arcs in Weyl semimetals: Lattice-based approach to the chiral anomaly, *Phys. Rev. B* **99**, 140201 (2019), arXiv:1807.06615 [cond-mat.mes-hall].
- [29] V. A. Kostelecký and C. D. Lane, Nonrelativistic quantum Hamiltonian for Lorentz violation, *J. Math. Phys.* **40**, 6245 (1999), arXiv:hep-ph/9909542.
- [30] R. Casana, M. M. Ferreira, Jr., V. E. Mouchrek-Santos, and E. O. Silva, Generation of geometrical phases and persistent spin currents in 1-dimensional rings by Lorentz-violating terms, *Phys. Lett. B* **746**, 171 (2015), arXiv:1504.06027 [hep-th].
- [31] H. Belich, T. Costa-Soares, M. M. Ferreira, Jr., and J. A. Helayël-Neto, Non-minimal coupling to a Lorentz-violating background and topological implications, *Eur. Phys. J. C* **41**, 421 (2005), arXiv:hep-th/0410104.
- [32] H. Belich, T. Costa-Soares, M. M. Ferreira, Jr., J. A. Helayël-Neto, and M. T. D. Orlando, A comment on the topological phase for anti-particles in a Lorentz-violating environment, *Phys. Lett. B* **639**, 675 (2006), arXiv:hep-th/0603091.
- [33] L. R. Ribeiro, E. Passos, C. Furtado, and J. R. Nascimento, Geometric phases modified by a Lorentz-symmetry violation background, *Int. J. Mod. Phys. A* **30**, 1550072 (2015), arXiv:0710.5858 [hep-th].
- [34] K. Bakke, H. Belich, and E. O. Silva, Relativistic Anandan quantum phase in the Lorentz violation background, *Annalen Phys.* **523**, 910 (2011).
- [35] H. Belich, E. O. Silva, M. M. Ferreira, Jr., and M. T. D. Orlando, Aharonov-Bohm-Casher Problem with a non-minimal Lorentz-violating coupling, *Phys. Rev. D* **83**, 125025 (2011), arXiv:1106.0789 [hep-th].
- [36] K. Bakke, E. O. Silva, and H. Belich, He-McKellar-Wilkens effect and scalar Aharonov-Bohm effect for a neutral particle based on the Lorentz symmetry violation, *J. Phys. G* **39**, 055004 (2012), arXiv:1203.3407 [hep-th].
- [37] K. Bakke and H. Belich, Abelian geometric phase for a Dirac neutral particle in a Lorentz symmetry violation environment, *J. Phys. G* **39**, 085001 (2012), arXiv:1206.2249 [hep-th].
- [38] K. Bakke and H. Belich, Quantum holonomies based on the Lorentz-violating tensor background, *J. Phys. G* **40**, 065002 (2013), arXiv:1304.4833 [hep-th].
- [39] A. G. de Lima, H. Belich, and K. Bakke, Anandan quantum phase and quantum holonomies induced by the effects of the Lorentz symmetry violation background in the CPT-even gauge sector of the Standard Model Extension, *Eur. Phys. J. Plus* **128**, 154 (2013).
- [40] K. Bakke and H. Belich, Relativistic geometric quantum phases from the Lorentz symmetry violation effects in the CPT-even gauge sector of Standard Model Extension, *Int. J. Mod. Phys. A* **30**, 1550197 (2015), arXiv:1412.5080 [hep-th].
- [41] K. Bakke and H. Belich, Aharonov-Anandan quantum phase from a fixed vector field background and an axial magnetic field around a cavity, *Quant. Stud. Math. Found.* **12**, 4 (2025).
- [42] V. A. Kostelecký and N. Russell, Data tables for Lorentz and CPT violation, *Rev. Mod. Phys.* **83**, 11 (2011), arXiv:0801.0287 [hep-ph].
- [43] R. Bluhm, Overview of the Standard Model Extension: Implications and phenomenology of Lorentz violation, in *Special Relativity. Will it Survive the Next 101 Years?*, Lect. Notes Phys., Vol. 702 (Springer, Berlin · Heidelberg, 2006) pp. 191–226, J. Ehlers and C. Lämmerzahl ed., arXiv:hep-ph/0506054.
- [44] J. D. Tasson, What do we know about Lorentz invariance?, *Rept. Prog. Phys.* **77**, 062901 (2014), arXiv:1403.7785 [hep-ph].
- [45] C. M. Will, The confrontation between general relativity and experiment, *Living Rev. Rel.* **17**, 4 (2014), arXiv:1403.7377 [gr-qc].
- [46] A. Hees, Q. G. Bailey, A. Bourgoin, H. P.-L. Bars, C. Guerlin, and C. Le Poncin-Lafitte, Tests of Lorentz symmetry in the gravitational sector, *Universe* **2**, 30 (2016), arXiv:1610.04682 [gr-qc].
- [47] Á. Roberts, Astrophysical neutrinos in testing Lorentz symmetry, *Galaxies* **9**, 47 (2021).
- [48] Q. G. Bailey, Testing gravity in the laboratory, in *Recent Progress on Gravity Tests: Challenges and Future Perspectives* (Springer, Singapore, 2024) pp. 1–26, C. Bambi and A. Cárdenas-Avendaño ed., arXiv:2305.06325 [gr-qc].
- [49] R. Jackiw and V. A. Kostelecký, Radiatively induced Lorentz and CPT violation in electrodynamics, *Phys. Rev. Lett.* **82**, 3572 (1999), arXiv:hep-ph/9901358.
- [50] M. Pérez-Victoria, Exact calculation of the radiatively induced Lorentz and CPT violation in QED, *Phys. Rev. Lett.* **83**, 2518 (1999), arXiv:hep-th/9905061.
- [51] J.-M. Chung and P. Oh, Lorentz and CPT violating Chern-Simons term in the derivative expansion of QED, *Phys. Rev. D* **60**, 067702 (1999), arXiv:hep-th/9812132.
- [52] J.-M. Chung, Radiatively-induced Lorentz and CPT violating Chern-Simons term in QED, *Phys. Lett. B* **461**, 138 (1999), arXiv:hep-th/9905095.
- [53] J.-M. Chung, Lorentz- and CPT-violating Chern-Simons term in the functional integral formalism, *Phys. Rev. D* **60**, 127901 (1999), arXiv:hep-th/9904037.
- [54] V. A. Kostelecký, C. D. Lane, and A. G. M. Pickering, One-loop renormalization of Lorentz-violating electrodynamics, *Phys. Rev. D* **65**, 056006 (2002), arXiv:hep-th/0111123.
- [55] B. Altschul, Failure of gauge invariance in the non-perturbative formulation of massless Lorentz-violating QED, *Phys. Rev. D* **69**, 125009 (2004), arXiv:hep-th/0311200.

- [56] B. Altschul, Gauge invariance and the Pauli-Villars regulator in Lorentz- and CPT-violating electrodynamics, *Phys. Rev. D* **70**, 101701(R) (2004), arXiv:hep-th/0407172.
- [57] R. Lehnert, Dirac theory within the Standard-Model Extension, *J. Math. Phys.* **45**, 3399 (2004), arXiv:hep-ph/0401084.
- [58] B. Altschul and D. Colladay, Velocity in Lorentz-violating fermion theories, *Phys. Rev. D* **71**, 125015 (2005), arXiv:hep-th/0412112.
- [59] B. Altschul and V. A. Kostelecký, Spontaneous Lorentz violation and nonpolynomial interactions, *Phys. Lett. B* **628**, 106 (2005), arXiv:hep-th/0509068.
- [60] R. Lehnert, Nonlocal on-shell field redefinition for the standard-model extension, *Phys. Rev. D* **74**, 125001 (2006), arXiv:hep-th/0609162.
- [61] A. P. Baêta Scarpelli, M. Sampaio, M. C. Nemes, and B. Hiller, Gauge invariance and the CPT and Lorentz violating induced Chern–Simons-like term in extended QED, *Eur. Phys. J. C* **56**, 571 (2008), arXiv:0804.3537 [hep-th].
- [62] V. A. Kostelecký and M. Mewes, Fermions with Lorentz-violating operators of arbitrary dimension, *Phys. Rev. D* **88**, 096006 (2013), arXiv:1308.4973 [hep-ph].
- [63] A. P. Baeta Scarpelli, T. Mariz, J. R. Nascimento, and A. Yu. Petrov, Four-dimensional aether-like Lorentz-breaking QED revisited and problem of ambiguities, *Eur. Phys. J. C* **73**, 2526 (2013), arXiv:1304.2256 [hep-th].
- [64] J. F. Assunção, T. Mariz, and A. Yu. Petrov, Non-analyticity of the induced Carroll-Field-Jackiw term at finite temperature, *EPL* **116**, 31003 (2016), arXiv:1609.09120 [hep-th].
- [65] J. A. A. S. Reis and M. Schreck, Lorentz-violating modification of Dirac theory based on spin-nondegenerate operators, *Phys. Rev. D* **95**, 075016 (2017), arXiv:1612.06221 [hep-th].
- [66] V. A. Kostelecký and Z. Li, Gauge field theories with Lorentz-violating operators of arbitrary dimension, *Phys. Rev. D* **99**, 056016 (2019), arXiv:1812.11672 [hep-ph].
- [67] A. F. Ferrari, J. R. Nascimento, and A. Yu. Petrov, Radiative corrections and Lorentz violation, *Eur. Phys. J. C* **80**, 459 (2020), arXiv:1812.01702 [hep-th].
- [68] B. Gonçalves, M. M. Dias Júnior, and B. J. Ribeiro, Exact Foldy-Wouthuysen transformation for a Dirac theory revisited, *Phys. Rev. D* **99**, 096015 (2019), arXiv:1812.11657 [hep-th].
- [69] A. Gómez, A. Martín-Ruiz, and L. F. Urrutia, Effective electromagnetic actions for Lorentz violating theories exhibiting the axial anomaly, *Phys. Lett. B* **829**, 137043 (2022), arXiv:2201.09420 [hep-th].
- [70] V. A. Kostelecký and N. Russell, Classical kinematics for Lorentz violation, *Phys. Lett. B* **693**, 443 (2010), arXiv:1008.5062 [hep-ph].
- [71] V. A. Kostelecký, Riemann-Finsler geometry and Lorentz-violating kinematics, *Phys. Lett. B* **701**, 137 (2011), arXiv:1104.5488 [hep-th].
- [72] V. A. Kostelecký, N. Russell, and R. Tso, Bipartite Riemann–Finsler geometry and Lorentz violation, *Phys. Lett. B* **716**, 470 (2012), arXiv:1209.0750 [hep-th].
- [73] M. A. Javaloyes and M. Sánchez, Finsler metrics and relativistic spacetimes, *Int. J. Geom. Meth. Mod. Phys.* **11**, 1460032 (2014), arXiv:1311.4770 [math.DG].
- [74] D. Colladay and P. McDonald, Singular Lorentz-violating Lagrangians and associated Finsler structures, *Phys. Rev. D* **92**, 085031 (2015), arXiv:1507.01018 [hep-ph].
- [75] J. Foster and R. Lehnert, Classical-physics applications for Finsler b space, *Phys. Lett. B* **746**, 164 (2015), arXiv:1504.07935 [physics.class-ph].
- [76] D. Colladay, Extended hamiltonian formalism and Lorentz-violating lagrangians, *Phys. Lett. B* **772**, 694 (2017), arXiv:1706.06637 [hep-th].
- [77] J. E. G. Silva, R. V. Maluf, and C. A. S. Almeida, Bipartite-Finsler symmetries, *Phys. Lett. B* **798**, 135009 (2019), arXiv:1907.11214 [gr-qc].
- [78] J. F. Davis, B. R. Edwards, and V. A. Kostelecký, Characteristic tensors for almost Finsler manifolds, arXiv:2508.21744 [math.DG] (2025).
- [79] R. Bluhm, V. A. Kostelecký, and N. Russell, CPT and Lorentz tests in hydrogen and antihydrogen, *Phys. Rev. Lett.* **82**, 2254 (1999), arXiv:hep-ph/9810269.
- [80] R. Bluhm and V. A. Kostelecký, Lorentz and CPT tests with spin-polarized solids, *Phys. Rev. Lett.* **84**, 1381 (2000), arXiv:hep-ph/9912542.
- [81] R. Bluhm, V. A. Kostelecký, and C. D. Lane, CPT and Lorentz tests with muons, *Phys. Rev. Lett.* **84**, 1098 (2000), arXiv:hep-ph/9912451.
- [82] V. A. Kostelecký and C. D. Lane, Constraints on Lorentz violation from clock-comparison experiments, *Phys. Rev. D* **60**, 116010 (1999), arXiv:hep-ph/9908504.
- [83] R. K. Mittleman, I. I. Ioannou, H. G. Dehmelt, and N. Russell, Bound on CPT and Lorentz symmetry with a trapped electron, *Phys. Rev. Lett.* **83**, 2116 (1999).
- [84] H. Dehmelt, R. Mittleman, R. S. Van Dyck, Jr., and P. Schwinberg, Past electron-positron $g-2$ experiments yielded sharpest bound on CPT violation for point particles, *Phys. Rev. Lett.* **83**, 4694 (1999), arXiv:hep-ph/9906262.
- [85] D. Bear, R. E. Stoner, R. L. Walsworth, V. A. Kostelecký, and C. D. Lane, Limit on Lorentz and CPT violation of the neutron using a two-species noble-gas maser, *Phys. Rev. Lett.* **85**, 5038 (2000), [Erratum: *Phys. Rev. Lett.* **89**, 209902 (2002)], arXiv:physics/0007049.
- [86] D. F. Phillips, M. A. Humphrey, E. M. Mattison, R. E. Stoner, R. F. C. Vessot, and R. L. Walsworth, Limit on Lorentz and CPT violation of the proton using a hydrogen maser, *Phys. Rev. D* **63**, 111101 (2001), arXiv:physics/0008230.
- [87] M. A. Humphrey, D. F. Phillips, E. M. Mattison, R. F. C. Vessot, R. E. Stoner, and R. L. Walsworth, Testing CPT and Lorentz symmetry with hydrogen masers, *Phys. Rev. A* **68**, 063807 (2003), arXiv:physics/0103068.
- [88] M. Deile *et al.* (Muon $g-2$), Testing CPT and Lorentz invariance with the anomalous spin precession of the muon, in *Proceedings of the Second Meeting on CPT and Lorentz Symmetry*, edited by V. A. Kostelecký (World Scientific Publishing, Singapore, 2002) pp. 305–310, arXiv:hep-ex/0110044.
- [89] V. W. Hughes, M. Grosse Perdekamp, D. Kawall, W. Liu, K. Jungmann, and G. zu Putlitz, Test of CPT and Lorentz invariance from muonium spectroscopy, *Phys. Rev. Lett.* **87**, 111804 (2001), arXiv:hep-ex/0106103.
- [90] L.-S. Hou, W.-T. Ni, and Y.-C. M. Li, Test of cosmic spatial isotropy for polarized electrons using a rotatable

- torsion balance, Phys. Rev. Lett. **90**, 201101 (2003), arXiv:physics/0009012.
- [91] B. R. Heckel, C. E. Cramer, T. S. Cook, E. G. Adelberger, S. Schlamminger, and U. Schmidt, New CP-violation and preferred-frame tests with polarized electrons, Phys. Rev. Lett. **97**, 021603 (2006), arXiv:hep-ph/0606218.
- [92] G. W. Bennett *et al.* (Muon g-2), Search for Lorentz and CPT violation effects in muon spin precession, Phys. Rev. Lett. **100**, 091602 (2008), arXiv:0709.4670 [hep-ex].
- [93] B. R. Heckel, E. G. Adelberger, C. E. Cramer, T. S. Cook, S. Schlamminger, and U. Schmidt, Preferred-frame and CP-violation tests with polarized electrons, Phys. Rev. D **78**, 092006 (2008), arXiv:0808.2673 [hep-ex].
- [94] I. Altarev *et al.*, Test of Lorentz invariance with spin precession of ultracold neutrons, Phys. Rev. Lett. **103**, 081602 (2009), arXiv:0905.3221 [nucl-ex].
- [95] J. M. Brown, S. J. Smullin, T. W. Kornack, and M. V. Romalis, New limit on Lorentz- and CPT-violating neutron spin interactions, Phys. Rev. Lett. **105**, 151604 (2010), arXiv:1006.5425 [physics.atom-ph].
- [96] C. Gemmel *et al.*, Limit on Lorentz and CPT violation of the bound neutron using a free precession $^3\text{He}/^{129}\text{Xe}$ comagnetometer, Phys. Rev. D **82**, 111901 (2010), arXiv:1011.2143 [gr-qc].
- [97] S. K. Peck, D. K. Kim, D. Stein, D. Orbaker, A. Foss, M. T. Hummon, and L. R. Hunter, Limits on local Lorentz invariance in mercury and cesium, Phys. Rev. A **86**, 012109 (2012), arXiv:1205.5022 [physics.atom-ph].
- [98] A. Fittante and N. Russell, Fermion observables for Lorentz violation, J. Phys. G **39**, 125004 (2012), arXiv:1210.2003 [hep-ph].
- [99] F. Allmendinger, W. Heil, S. Karpuk, W. Kilian, A. Scharth, U. Schmidt, A. Schnabel, Yu. Sobolev, and K. Tullney, New limit on Lorentz-invariance- and CPT-violating neutron spin interactions using a free-spin-precession $^3\text{He}-^{129}\text{Xe}$ comagnetometer, Phys. Rev. Lett. **112**, 110801 (2014), arXiv:1312.3225 [gr-qc].
- [100] B. M. Roberts, Y. V. Stadnik, V. A. Dzuba, V. V. Flambaum, N. Leefer, and D. Budker, Limiting P-odd interactions of cosmic fields with electrons, protons and neutrons, Phys. Rev. Lett. **113**, 081601 (2014), arXiv:1404.2723 [hep-ph].
- [101] Y. V. Stadnik and V. V. Flambaum, Nuclear spin-dependent interactions: Searches for WIMP, axion and topological defect dark matter, and tests of fundamental symmetries, Eur. Phys. J. C **75**, 110 (2015), arXiv:1408.2184 [hep-ph].
- [102] A. H. Gomes, V. A. Kostelecký, and A. J. Vargas, Laboratory tests of Lorentz and CPT symmetry with muons, Phys. Rev. D **90**, 076009 (2014), arXiv:1407.7748 [hep-ph].
- [103] J. P. Noordmans, C. J. G. Onderwater, H. W. Wilschut, and R. G. E. Timmermans, Question of Lorentz violation in muon decay, Phys. Rev. D **93**, 116001 (2016), arXiv:1412.3257 [hep-ph].
- [104] B. M. Roberts, Y. V. Stadnik, V. A. Dzuba, V. V. Flambaum, N. Leefer, and D. Budker, Parity-violating interactions of cosmic fields with atoms, molecules, and nuclei: Concepts and calculations for laboratory searches and extracting limits, Phys. Rev. D **90**, 096005 (2014), arXiv:1409.2564 [hep-ph].
- [105] M. S. Berger, V. A. Kostelecký, and Z. Liu, Lorentz and CPT violation in top-quark production and decay, Phys. Rev. D **93**, 036005 (2016), arXiv:1509.08929 [hep-ph].
- [106] V. A. Kostelecký and A. J. Vargas, Lorentz and CPT tests with hydrogen, antihydrogen, and related systems, Phys. Rev. D **92**, 056002 (2015), arXiv:1506.01706 [hep-ph].
- [107] Y. Ding and V. A. Kostelecký, Lorentz-violating spinor electrodynamics and Penning traps, Phys. Rev. D **94**, 056008 (2016), arXiv:1608.07868 [hep-ph].
- [108] C. Smorra *et al.* (BASE), A parts-per-billion measurement of the antiproton magnetic moment, Nature **550**, 371 (2017).
- [109] H. Nagahama *et al.* (BASE), Sixfold improved single particle measurement of the magnetic moment of the antiproton, Nature Commun. **8**, 14084 (2017).
- [110] C. A. Escobar, J. P. Noordmans, and R. Potting, Cosmic-ray fermion decay through tau-antitau emission with Lorentz violation, Phys. Rev. D **97**, 115030 (2018), arXiv:1804.07586 [hep-ph].
- [111] C. Smorra *et al.*, Direct limits on the interaction of antiprotons with axion-like dark matter, Nature **575**, 310 (2019), arXiv:2006.00255 [physics.atom-ph].
- [112] Y. Ding, Lorentz and CPT tests using Penning traps, Symmetry **11**, 1220 (2019), arXiv:1910.00456 [hep-ph].
- [113] C. Smorra and A. Mooser, Precision measurements of the fundamental properties of the proton and antiproton, J. Phys. Conf. Ser. **1412**, 032001 (2020), arXiv:2002.04261 [physics.atom-ph].
- [114] Y. Ding and M. F. Rawnak, Lorentz and CPT tests with charge-to-mass ratio comparisons in Penning traps, Phys. Rev. D **102**, 056009 (2020), arXiv:2008.08484 [hep-ph].
- [115] A. J. Acevedo-López, Y. Ding, K. Iwasaki, and A. J. Vargas, Lorentz- and CPT-violating effects in Penning traps at linear boost, Phys. Rev. D **108**, 076014 (2023), arXiv:2308.14201 [hep-ph].
- [116] A. Belyaev, L. Cerrito, E. Lunghi, S. Moretti, and N. Sherrill, Probing CPT invariance with top quarks at the LHC, Phys. Rev. Lett. **133**, 221601 (2024), arXiv:2405.12162 [hep-ph].
- [117] A. A. Zyuzin, S. Wu, and A. A. Burkov, Weyl semimetal with broken time reversal and inversion symmetries, Phys. Rev. B **85**, 165110 (2012), arXiv:1201.3624 [cond-mat.mes-hall].
- [118] K. Landsteiner, Y. Liu, and Y.-W. Sun, Quantum phase transition between a topological and a trivial semimetal from holography, Phys. Rev. Lett. **116**, 081602 (2016), arXiv:1511.05505 [hep-th].
- [119] K. Koepnick, D. Kasinathan, D. V. Efremov, S. Khim, S. Borisenko, B. Büchner, and J. van den Brink, TaIrTe_4 : A ternary type-II Weyl semimetal, Phys. Rev. B **93**, 201101(R) (2016).
- [120] J. Ruan, S.-K. Jian, D. Zhang, H. Yao, H. Zhang, S.-C. Zhang, and D. Xing, Ideal Weyl semimetals in the chalcopyrites CuTiSe_2 , AgTiTe_2 , AuTiTe_2 , and ZnPbAs_2 , Phys. Rev. Lett. **116**, 226801 (2016).
- [121] X.-B. Wang, X.-M. Ma, E. Emmanouilidou, B. Shen, C.-H. Hsu, C.-S. Zhou, Y. Zuo, R.-R. Song, S.-Y. Xu, G. Wang, L. Huang, N. Ni, and C. Liu, Topological surface electronic states in candidate nodal-line semimetal CaAgAs , Phys. Rev. B **96**, 161112 (2017).
- [122] Y. J. Jin, R. Wang, Z. J. Chen, J. Z. Zhao, Y. J. Zhao, and H. Xu, Ferromagnetic Weyl semimetal phase in a

- tetragonal structure, Phys. Rev. B **96**, 201102 (2017).
- [123] B. Q. Lv, T. Qian, and H. Ding, Experimental perspective on three-dimensional topological semimetals, Rev. Mod. Phys. **93**, 025002 (2021).
 - [124] D. Colladay and P. McDonald, Classical Lagrangians for momentum dependent Lorentz violation, Phys. Rev. D **85**, 044042 (2012), arXiv:1201.3931 [hep-ph].
 - [125] N. Russell, Finsler-like structures from Lorentz-breaking classical particles, Phys. Rev. D **91**, 045008 (2015), arXiv:1501.02490 [hep-th].
 - [126] J. A. A. S. Reis and M. Schreck, Leading-order classical Lagrangians for the nonminimal Standard-Model extension, Phys. Rev. D **97**, 065019 (2018), arXiv:1711.11169 [hep-th].
 - [127] J. A. A. S. Reis and M. Schreck, Formal developments for Lorentz-violating Dirac fermions and neutrinos, Symmetry **11**, 1197 (2019), arXiv:1909.11061 [hep-th].
 - [128] J. A. A. S. Reis and M. Schreck, Classical Lagrangians for the nonminimal spin-nondegenerate Standard-Model extension at higher orders in Lorentz violation, Phys. Rev. D **103**, 095029 (2021), arXiv:2102.10164 [hep-th].
 - [129] F. Canè, D. Bear, D. F. Phillips, M. S. Rosen, C. L. Smallwood, R. E. Stoner, R. L. Walsworth, and V. A. Kostelecký, Bound on Lorentz and CPT violating boost effects for the neutron, Phys. Rev. Lett. **93**, 230801 (2004), arXiv:physics/0309070.
 - [130] B. Altschul, Bounds on spin-dependent Lorentz violation from inverse Compton observations, Phys. Rev. D **75**, 041301 (2007), arXiv:hep-ph/0612288.
 - [131] B. Altschul, Disentangling forms of Lorentz violation with complementary clock comparison experiments, Phys. Rev. D **79**, 061702 (2009), arXiv:0901.1870 [hep-ph].
 - [132] V. M. Abazov *et al.* (D0), Search for violation of Lorentz invariance in top quark pair production and decay, Phys. Rev. Lett. **108**, 261603 (2012), arXiv:1203.6106 [hep-ex].
 - [133] M. Schreck, Vacuum Cherenkov radiation for Lorentz-violating fermions, Phys. Rev. D **96**, 095026 (2017), arXiv:1702.03171 [hep-ph].
 - [134] E. Lunghi, N. Sherrill, A. Szczepaniak, and A. Vieira, Quark-sector Lorentz violation in Z -boson production, JHEP **04** (2021), 228, [Erratum: JHEP **07** (2024) 167(E)], arXiv:2011.02632 [hep-ph].
 - [135] D. S. Cabral and A. F. Santos, Exploring the impact of magnetic fields, Lorentz violation and EDM on $e^+e^- \rightarrow l^+l^-$ scattering, Eur. Phys. J. Plus **139**, 789 (2024), arXiv:2408.16790 [hep-ph].
 - [136] S. Aghababaei, Constraints on Lorentz violation parameter through electric dipole moments, Eur. Phys. J. C **84**, 173 (2024).
 - [137] T. T. Wu and C. N. Yang, Concept of nonintegrable phase factors and global formulation of gauge fields, Phys. Rev. D **12**, 3845 (1975).
 - [138] D. Colladay and V. A. Kostelecký, Cross sections and lorentz violation, Phys. Lett. B **511**, 209 (2001), arXiv:hep-ph/0104300.
 - [139] F. R. Klinkhamer and G. E. Volovik, Emergent CPT violation from the splitting of Fermi points, Int. J. Mod. Phys. A **20**, 2795 (2005), arXiv:hep-th/0403037.
 - [140] G. E. Volovik, *The Universe in a Helium Droplet*, International Series of Monographs on Physics, Vol. 117 (Oxford University Press, New York (NY), USA, 2003).
 - [141] R. Bluhm, V. A. Kostelecký, C. D. Lane, and N. Russell, Probing Lorentz and CPT violation with space-based experiments, Phys. Rev. D **68**, 125008 (2003), arXiv:hep-ph/0306190.
 - [142] R. Bluhm, V. A. Kostelecký, C. D. Lane, and N. Russell, Clock-comparison tests of Lorentz and CPT symmetry in space, Phys. Rev. Lett. **88**, 090801 (2002), arXiv:hep-ph/0111141.
 - [143] V. A. Kostelecký and M. Mewes, Signals for Lorentz violation in electrodynamics, Phys. Rev. D **66**, 056005 (2002), arXiv:hep-ph/0205211.
 - [144] V. A. Kostelecký, Sensitivity of CPT tests with neutral mesons, Phys. Rev. Lett. **80**, 1818 (1998), arXiv:hep-ph/9809572.